

The dissipation tensor ε_{ij} in wall turbulence

G. A. GEROLYMOS, I. VALLET[†]

Sorbonne Universités, Université Pierre-et-Marie-Curie (UPMC), 4 place Jussieu, 75005 Paris, France

(Received 14 September 2016)

The paper investigates the dissipation tensor ε_{ij} in wall turbulence. Available DNS data are examined to illustrate the differences in the anisotropy of the dissipation tensor ε_{ij} with respect to the anisotropy of the Reynolds-stresses r_{ij} . The budgets of the transport equations of the dissipation tensor ε_{ij} are studied using novel DNS data of low-Reynolds-number turbulent plane channel flow with spatial resolution sufficiently fine to accurately determine the correlations of products of 2-derivatives of fluctuating velocities u'_i and pressure p' which appear in various terms. Finally, the influence of the Reynolds number on the diagonal components of ε_{ij} (ε_{xx} , ε_{yy} , ε_{zz}) and on the various terms in their transport equations is studied using available DNS data of Vreman and Kuerten (*Phys. Fluids* **26** (2014) 085103).

Key words: wall-turbulence, Reynolds-stress, dissipation tensor, transport equations budgets

1. Introduction

The Reynolds-stress tensor $-\rho r_{ij}$ (where $r_{ij} := \overline{u'_i u'_j}$ are the 2-moments of the fluctuating velocity components, $u_i \in \{u, v, w\}$ are the velocity components in a Cartesian reference-frame $x_i \in \{x, y, z\}$, (\cdot) denotes Reynolds (ensemble) averaging and $(\cdot)'$ turbulent fluctuations around the mean-value) represents the influence of turbulent momentum-mixing on the mean-flow (Pope 2000, pp. 86–87). Throughout the paper we consider incompressible flow (with density $\rho \approx \text{const}$), in an inertial reference-frame (Speziale 1989), with a Newtonian constitutive relation for the viscous stresses (Davidson 2004, (2.4), p. 31), and we assume that the variations of dynamic viscosity are negligible ($\mu \approx \text{const}$). The exact equation for the transport of r_{ij} (Pope 2000, (7.178–7.181), p. 315)

$$\underbrace{\rho \frac{\partial \overline{u'_i u'_j}}{\partial t} + \rho \bar{u}_\ell \frac{\partial \overline{u'_i u'_j}}{\partial x_\ell}}_{C_{ij}} = \underbrace{\frac{\partial}{\partial x_\ell} \left(\mu \frac{\partial \overline{u'_i u'_j}}{\partial x_\ell} \right)}_{d_{ij}^{(\mu)}} + \underbrace{\frac{\partial}{\partial x_\ell} \left(-\rho \overline{u'_i u'_j u'_\ell} \right)}_{d_{ij}^{(u)}} + \underbrace{\left(-\overline{u'_i \frac{\partial p'}{\partial x_j}} - \overline{u'_j \frac{\partial p'}{\partial x_i}} \right)}_{\Pi_{ij}} + \underbrace{\left(-\rho \overline{u'_i u'_\ell} \frac{\partial \bar{u}_j}{\partial x_\ell} - \rho \overline{u'_j u'_\ell} \frac{\partial \bar{u}_i}{\partial x_\ell} \right)}_{P_{ij}} - \underbrace{\left(2\mu \frac{\partial \overline{u'_i}}{\partial x_\ell} \frac{\partial \overline{u'_j}}{\partial x_\ell} \right)}_{\rho \varepsilon_{ij}} \quad (1.1)$$

states that the convection of r_{ij} by the mean-velocity field C_{ij} is the balance of 5 mechanisms: diffusion by molecular viscosity $d_{ij}^{(\mu)}$, diffusion by the fluctuating-velocity field $d_{ij}^{(u)}$, interaction of the fluctuating velocity with the fluctuating pressure-gradient Π_{ij} ,

[†] Email address for correspondence: isabelle.vallet@upmc.fr

production by the interaction of the Reynolds-stresses with mean velocity-gradients P_{ij} , and destruction by molecular friction $-\rho\varepsilon_{ij}$. Notice that deterministic body-forces (eg gravity in incompressible flow) do not appear in (1.1) (ie do not influence directly r_{ij}). Budgets of (1.1) in wall-turbulence have been studied via DNS (Kim 2012) by various authors, for plane channel (Mansour, Kim & Moin 1988; Moser, Kim & Mansour 1999), pipe (Khoury, Schlatter, Noorani, Fischer, Brethouwer & Johansson 2013) or boundary-layer (Sillero, Jiménez & Moser 2013) flows. On the other hand, although the dissipation tensor

$$\varepsilon_{ij} := 2\nu \overline{\frac{\partial u'_i}{\partial x_\ell} \frac{\partial u'_j}{\partial x_\ell}} \quad (1.2a)$$

has been examined (Mansour *et al.* 1988) as part of the budgets of (1.1), and with respect to its anisotropy (Lai & So 1990; Jovanović, Ye & Durst 1995), to the authors knowledge, the transport equations for ε_{ij} in wall turbulence have not been studied in detail. Instead, attention has concentrated on its half-trace

$$\varepsilon := \frac{1}{2}\varepsilon_{mm} \stackrel{(1.2a)}{=} \nu \overline{\frac{\partial u'_m}{\partial x_\ell} \frac{\partial u'_m}{\partial x_\ell}} > 0 \quad (1.2b)$$

which represents the dissipation-rate of the turbulent kinetic energy $k := \frac{1}{2}r_{mm}$ and is strictly positive being the average of a sum of squares of real numbers (Schumann 1977). In (1.2) $\nu := \rho^{-1}\mu$ is the kinematic viscosity. Notice that although most authors (Mansour *et al.* 1988; Lai & So 1990; Speziale & Gatski 1997; Moser *et al.* 1999; Pope 2000; Jakirlić & Hanjalić 2002; Hoyas & Jiménez 2008) use definition (1.2a) for ε_{ij} , there are some workers in the field (Jovanović *et al.* 1995; Oberlack 1997) who do not include the factor 2 in (1.2a), with corresponding absence of the factor $\frac{1}{2}$ in (1.2b).

In an important early work, Lee & Reynolds (1987) analysed their DNS computations of homogeneous turbulence (distorted by different types of strain and at different nondimensional mean strain-rates $2k\varepsilon^{-1}\sqrt{\frac{1}{2}\overline{S_{ij}S_{ij}}}$ and then left unstrained to relax) using AIM (anisotropy invariant mapping) of the 2-moment tensors of the fluctuating fields of velocity $r_{ij} := \overline{u'_i u'_j}$, dissipation ε_{ij} (1.2b) and vorticity (Davidson 2004, $\vec{\omega} := \text{rot}\vec{V}$, pp. 39-50) $\overline{\omega'_i \omega'_j}$, with the underlying idea that $\overline{u'_i u'_j}$ characterizes the anisotropy of the large structures whereas ε_{ij} and $\overline{\omega'_i \omega'_j}$ measure the anisotropy of the small scales. They concluded that in the distortion phase "the vorticity field $\overline{\omega'_i \omega'_j}$ is always more anisotropic than the velocity field $\overline{u'_i u'_j}$ " (Lee & Reynolds 1987, p. 60) and that in the relaxation-phase "the large-scale anisotropy is also coupled with the small-scale turbulence" (Lee & Reynolds 1987, p. 66). Durbin & Speziale (1991) also considered ε_{ij} (1.2b) as the representative "small-scale statistic" and disproved (in an informal but plausible analysis by contradiction) the idea of local small-scale isotropy when the large scales are subjected to high nondimensional mean strain-rates, independently of the Reynolds number. Oberlack (1997) reviews different experimental and computational results concluding that "DNS have revealed the strong nonisotropic nature of the dissipation process", and that "a finite level of small-scale anisotropy must always exist if the large scales are anisotropic". In such situations of highly anisotropic ε_{ij} "the small scales are not dominated by a classical energy cascade" (Bhattacharya *et al.* 2008, p. 9). The importance of the small-scale anisotropy represented by the anisotropy of ε_{ij} (1.2b) is central in the modelling work of Speziale & Gatski (1997) and Lumley *et al.* (1999). In an early work, Tagawa, Nagano & Tsuji (1991) developed a 12-equation r_{ij} - ε_{ij} closure to improve near-wall modelling.

Wall turbulence is much more complex, not only because of the strong inhomogeneity

in the wall-normal direction which is induced by the mean-flow field (Buschmann & Gad-el-Hak 2007), but also because of the direct influence of the wall, which is twofold: on the one hand the no-slip boundary-condition imposes, at the wall, a 2-C (Lumley 1978; Simonsen & Krogstad 2005, 2-component) componentality (Kassinos *et al.* 2001) both on the 2-moments of the fluctuating velocities $r_{ij} := \overline{u'_i u'_j}$ (Mansour *et al.* 1988, Fig. 17, p. 32) and on the dissipation tensor ε_{ij} (Mansour *et al.* 1988, Fig. 18, p. 32), and on the other hand wall-echo (Kim 1989; Chang, Piomelli & Blake 1999; Gerolymos, S  n  chal & Vallet 2013) strongly impacts the fluctuating-pressure field.

Mansour *et al.* (1988) presented for the first time, in incompressible fully developed (streamwise invariant in the mean) plane channel flow, the budgets of the transport equation for ε (1.2b), which had "*eluded measurement techniques*". The analysis of Mansour *et al.* (1988) reveals the specific behaviour of the 4 different production mechanisms of ε (Mansour *et al.* 1988, (23), p. 23), and DNS data show (Mansour *et al.* 1988, Fig. 6, p. 24) that all of these mechanisms are of comparable importance near the wall (inner-scaled wall-distance $y^+ \lesssim 15$), except for the production by the mean-velocity Hessian $P_\varepsilon^{(3)} := -2\rho\nu\overline{u'_k \partial_{x_j} u'_i \partial_{x_k x_j}^2 \bar{u}_i}$ (Mansour *et al.* 1988, (23), p. 23) which is generally weaker. On the other hand, further away from the wall ($y^+ \gtrsim 30$) the production by the triple correlations of the fluctuating velocity-gradients $P_\varepsilon^{(4)} := -2\rho\nu\overline{\partial_{x_k} u'_i \partial_{x_j} u'_i \partial_{x_j} u'_k}$ (Mansour *et al.* 1988, (23), p. 23) becomes the dominant ε -production mechanism. The predominance of $P_\varepsilon^{(4)}$ away from the wall is consistent with the quasi-homogeneous order-of-magnitude analysis of Tennekes & Lumley (1972, pp. 88–92) which concludes that the major production mechanism of the fluctuating vorticity $\omega'_i \omega'_i$ is $\rho\overline{\omega'_i \omega'_j S'_{ij}}$ (where $S_{ij} := \frac{1}{2}(\partial_{x_j} u_i + \partial_{x_i} u_j)$ is the strain-rate tensor) in line with Taylor (1938). Near the wall, the main hypothesis of this order-of-magnitude analysis (Tennekes & Lumley 1972, pp. 88–92), *viz* that the lengthscale characterizing the mean velocity-gradients is much larger than some appropriately defined microscale (Taylor 1938; Kolovandin & Vatutin 1972; Vreman & Kuerten 2014a) characterizing the fluctuating velocity-gradients, obviously breaks down (Vreman & Kuerten 2014a, Fig. 7, p. 15): "*near walls ... the scales of energy containing motions and the scales of dissipative motions are the same*" (Rodi & Mansour 1993, p. 510).

The wall-asymptotic (as $y^+ \rightarrow 0$) behaviour of various turbulent correlations can be studied by Taylor-series expansions (Riley *et al.* 2006, §4.6, pp. 136–141) in the wall-normal direction y^+ , in inner scaling (Buschmann & Gad-el-Hak 2007, \cdot^+), of the fluctuating velocities u_i^+ and fluctuating pressure p'^+ , under the constraints of the no-slip condition and of the Navier-Stokes equations. This procedure is described in Hinze (1975, pp. 620–621), and appears in a less systematic form (related to the mean-velocity expansion) in Townsend (1976, p. 163) and Monin & Yaglom (1971, p. 271). Chapman & Kuhn (1986) used this approach to resolve a controversy that existed at that time (Patel *et al.* 1985) concerning the asymptotic behaviour $-\overline{u'^+ v'^+} \propto y^{+3}$ of the turbulent shear stress near the wall ($y^+ \rightarrow 0$). Launder & Reynolds (1983) applied this technique to determine the wall-asymptotic behaviour of the components of the dissipation tensor ε_{ij} . Mansour *et al.* (1988) studied the wall-asymptotics of the various terms in the r_{ij} -transport budgets and in the budgets of the transport equation (Mansour *et al.* 1988, (23), p. 23) for the half-trace ε (1.2b). Hanjali   (1994, Tab. 3, p. 191) reported the wall-asymptotic expansions of the r_{ij} -anisotropy tensor $2b_{ij}$ (2.1a).

Jovanovi   *et al.* (1995) also focus on the transport equation for the half-trace ε (1.2b), arguing that the components of the dissipation tensor ε_{ij} can be "*analytically interpreted in terms of its trace $\varepsilon_{\ell\ell}$ and of the 2-point velocity correlations*". Using standard inhomogeneous 2-point-correlation techniques (Chou 1945, pp. 43–44), ε_{ij} (1.2a) is split into

an inhomogeneous part (which is $\frac{1}{2}\nu\nabla^2 r_{ij}$ and vanishes at the limit of homogeneous turbulence) and a quasi-homogeneous part which is always present. Jakirlić & Hanjalić (2002) modelled the unclosed terms in the corresponding equation for the homogeneous part of ε (1.2b), *viz* $\varepsilon - \frac{1}{2}\nu\nabla^2 k$, which they used in a Reynolds-stress 7-equation model framework, further developed and applied by Jakirlić *et al.* (2007) and Jakirlić & Maduta (2015).

Recently, Vreman & Kuerten (2014b) have studied using DNS the statistics, including skewness and flatness (Pope 2000, (3.37), p. 43) and pdfs (Pope 2000, probability-density functions, pp. 39–41) of the variance of the components of the fluctuating velocity-gradient $(\partial_{x_j} u'_i)^2$ and Hessian $(\partial_{x_j x_k}^2 u'_i)^2$, and of analogous correlations for the fluctuating pressure $((\partial_{x_i} p')^2, (\partial_{xx}^2 p')^2, (\partial_{yy}^2 p')^2, (\partial_{zz}^2 p')^2)$, in plane channel flow at friction Reynolds number (A 3g) $Re_{\tau_w} \approx 590$. They also analyzed the budgets of the transport equations for the 9 components $(\partial_{x_j} u'_i)^2$, which can be combined to obtain the transport equations for the diagonal components of ε_{ij} (1.2a), $\{\varepsilon_{xx}, \varepsilon_{yy}, \varepsilon_{zz}\}$. Correlations for the transport-equation budgets of the shear component ε_{xy} cannot be extracted from the data of Vreman & Kuerten (2014b). Near the wall, the shear component ε_{xy} is comparable with the wall-normal component ε_{yy} and should therefore be taken into account when studying the anisotropy of ε_{ij} (1.2a), and it has been argued (Hanjalić & Jakirlić 1993; Gerolymos, Lo, Vallet & Younis 2012b) that correct modelling of the shear component ε_{xy} is important in advanced RANS models. Furthermore, the results of the present work indicate that the ε_{xy} -budgets behave unlike those of the diagonal components, and such specific behaviour also applies to the relative importance of various mechanisms of production. An important observation of Vreman & Kuerten (2014b) is that the Laplacian $\nabla^2 p'$ is highly intermittent near the wall (Vreman & Kuerten 2014b, Fig. 12, p. 21) and this implies significant trailing tails in the corresponding pdfs (Vreman & Kuerten 2014b, Fig. 11, p. 20) and consequently very high values of flatness. Therefore correlations in the ε_{ij} -transport equations containing the components of the fluctuating pressure-Hessian $\partial_{x_j x_k}^2 p'$ require long observation times to reach statistical convergence. Vreman & Kuerten (2016) produced similar data in a highly resolved DNS at $Re_{\tau_w} \approx 180$.

The purpose of the paper is to study in detail the near-wall behaviour of the dissipation tensor ε_{ij} , using DNS data for incompressible low- Re_{τ_w} (friction Reynolds number) fully developed turbulent plane channel flow. The solver used to acquire these data was described in Gerolymos, Sénéchal & Vallet (2010) and uses an $O(\Delta\ell^{17})$ upwind-biased discretization for the convective terms (Gerolymos, Sénéchal & Vallet 2009). It has been validated by systematic (Gerolymos *et al.* 2010, 2013; Gerolymos & Vallet 2014) comparison with standard (Moser *et al.* 1999; del Álamo & Jiménez 2003; Hoyas & Jiménez 2006, 2008) DNS data (profiles, 2-point correlations and spectra in the homogeneous xz -directions, and r_{ij} -transport budgets), including assessment of the influence of compressibility at the low-Mach-number limit (Gerolymos *et al.* 2013, Appendix A, pp. 45–51). It should be stated from the outset that the present DNS data were obtained using a compressible airflow solver (Gerolymos *et al.* 2010), and computations were run at centerline Mach number $\bar{M}_{CL} = 0.35$. Specific comparisons with incompressible DNS data of Vreman & Kuerten (2014a,b, 2016) presented in §4 of the paper clearly demonstrate that the high-order statistics examined in the present work are not influenced by compressibility, at this $\bar{M}_{CL} = 0.35$.

In §2 we review existing DNS data concerning the anisotropy of r_{ij} (large scales) and ε_{ij} (small scales), in fully developed plane channel flow, including wall-asymptotics and the influence of Reynolds number, highlighting the main componentality differences between these 2 tensors. In §3 we present, to our knowledge for the first time, the budgets of

the transport equations (obtained by straightforward manipulations of the fluctuating continuity and momentum equations; §3.1) for all the components of ε_{ij} (including the shear component ε_{xy}), in low Reynolds number ($Re_{\tau_w} \approx 180$) plane channel flow. In §4 we use the data of Vreman & Kuerten (2014*a,b*, 2016), which can be combined to provide the budgets of the diagonal components of ε_{ij} (but not those of the shear component), both to assess the $Re_{\tau_w} \approx 180$ data and to discuss the evolution with Re_{τ_w} of different terms. Finally, in §5 we summarize the main new results obtained in the paper and discuss perspectives for future research.

2. DNS data for ε_{ij}

We consider fully developed turbulent plane channel flow, and use nondimensional inner variables (wall-units; §A.1). The channel height is 2δ , y is the wall-normal direction, x and z are, respectively, the streamwise and spanwise (crossflow) directions, along which mean-flow velocities and all turbulent moments are invariant. Available DNS databases (Kim *et al.* 1987; Moser *et al.* 1999; Hu *et al.* 2002, 2003, 2006; del Álamo & Jiménez 2003; Hoyas & Jiménez 2006, 2008; Lozano-Durán & Jiménez 2014; Bernardini *et al.* 2014; Vreman & Kuerten 2014*a,b*, 2016; Lee & Moser 2015) of turbulent plane channel flow provide information on the budgets of the r_{ij} -transport equations (1.1) which can be used to assess analogies and differences in the anisotropy of r_{ij} and ε_{ij} as the flow Reynolds number Re_{τ_w} (A 3*g*) varies.

2.1. Anisotropy

The traceless anisotropy tensor b_{ij} (Lumley 1978) and its invariants (Rivlin 1955) $\Pi_{\mathbf{b}}$ and $\text{III}_{\mathbf{b}}$ (Gerolymos *et al.* 2012*a*)

$$r_{ij} := \overline{u'_i u'_j} \quad ; \quad k := \frac{1}{2} \overline{u'_\ell u'_\ell} \quad ; \quad b_{ij} := \frac{\overline{u'_i u'_j}}{2k} - \frac{1}{3} \delta_{ij} \quad (2.1a)$$

$$\Pi_{\mathbf{b}} = -\frac{1}{2} b_{mk} b_{km} \quad ; \quad \text{III}_{\mathbf{b}} = \frac{1}{3} b_{mk} b_{kl} b_{lm} \quad ; \quad A := 1 + 27\text{III}_{\mathbf{b}} + 9\Pi_{\mathbf{b}} \quad (2.1b)$$

describe the local state of the Reynolds-stress tensor whose locus in the $(\text{III}_{\mathbf{b}}, -\Pi_{\mathbf{b}})$ -plane lies within Lumley's (1978) realisability triangle, determined by the fact (Schumann 1977) that the diagonal components ($r_{xx} := \overline{u'^2}$, $r_{yy} := \overline{v'^2}$, and $r_{zz} := \overline{w'^2}$) of the Reynolds-stress tensor \mathbf{r} are positive in any reference-frame (\mathbf{r} is positive-definite). The simplified form of $\Pi_{\mathbf{b}}$ and $\text{III}_{\mathbf{b}}$ in (2.1) takes into account that \mathbf{b} is traceless ($\mathbf{I}_{\mathbf{b}} = \text{tr} \mathbf{b} \stackrel{(2.1)}{=} 0$). In (2.1) $A \in [0, 1]$ is Lumley's (1978) flatness parameter which (Lumley 1978) tends to zero at the 2-component limit (Craft & Launder 2001, TCL), *ie* in the wall-turbulence case (Launder & Shima 1989) at the wall (inversely $A \rightarrow 0$ implies TCL).

The mathematical proof (Lumley 1978, pp. 138–140) that the invariants $\{\text{III}_{\mathbf{b}}, -\Pi_{\mathbf{b}}\}$ (2.1*b*) must lie within the realizability triangle only uses the condition that the diagonal components of the symmetric Reynolds-stress tensor \mathbf{r} ($r_{ij} := \overline{u'_i u'_j}$) are nonnegative for any orientation of the axes-of-coordinates (Schumann 1977) and hence also for the frame of the principal axes where the symmetric tensor \mathbf{r} is diagonalized (Aris 1962, pp. 25–28) with diagonal components its real eigenvalues. Since the eigenvalues of \mathbf{r} are real and nonnegative, \mathbf{r} is positive-definite (Stewart 1998, Theorem 2.3, p. 186). Therefore, the realizability triangle applies to the anisotropy invariants of any positive-definite symmetric order-2 tensor (equivalently any symmetric order-2 tensor whose diagonal elements are nonnegative for every orientation of the axes-of-coordinates). From definition (1.2*a*), the dissipation tensor ε is also positive-definite because its diagonal components ($\varepsilon_{xx} := 2\nu \partial_{x_\ell} u' \partial_{x_\ell} u'$, $\varepsilon_{yy} := 2\nu \partial_{x_\ell} v' \partial_{x_\ell} v'$, and $\varepsilon_{zz} := 2\nu \partial_{x_\ell} w' \partial_{x_\ell} w'$) are always positive.

Therefore, the corresponding traceless anisotropy tensor $b_{\varepsilon_{ij}}$ and its invariants (Rivlin 1955) $\Pi_{\mathbf{b}_\varepsilon}$ and $\text{III}_{\mathbf{b}_\varepsilon}$

$$\varepsilon_{ij} \stackrel{(1.2a)}{:=} 2\nu \frac{\partial u'_i}{\partial x_\ell} \frac{\partial u'_j}{\partial x_\ell} \quad ; \quad \varepsilon \stackrel{(1.2b)}{:=} \frac{1}{2} \varepsilon_{mm} \quad ; \quad b_{\varepsilon_{ij}} := \frac{\varepsilon_{ij}}{2\varepsilon} - \frac{1}{3} \delta_{ij} \quad (2.2a)$$

$$\Pi_{\mathbf{b}_\varepsilon} = -\frac{1}{2} b_{\varepsilon_{mk}} b_{\varepsilon_{km}} \quad ; \quad \text{III}_{\mathbf{b}_\varepsilon} = \frac{1}{3} b_{\varepsilon_{mk}} b_{\varepsilon_{k\ell}} b_{\varepsilon_{\ell m}} \quad ; \quad A_\varepsilon := 1 + 27\text{III}_{\mathbf{b}_\varepsilon} + 9\Pi_{\mathbf{b}_\varepsilon} \quad (2.2b)$$

define the same realizability triangle as \mathbf{b} (Lumley 1978; Simonsen & Krogstad 2005). This was first recognized by Lee & Reynolds (1987, p. 56), who also state regarding the invariants (2.1b, 2.2b) that "each AIM (anisotropy invariant mapping) has the boundaries first defined by Lumley & Newman (1977) for the Reynolds-stress AIM".

Since isotropy of r_{ij} (ε_{ij}) corresponds to $\mathbf{b} = 0$ ($\mathbf{b}_\varepsilon = 0$), the larger the distance of the components b_{ij} ($b_{\varepsilon_{ij}}$) from 0 the higher the anisotropy (Simonsen & Krogstad 2005).

2.2. Wall asymptotics

Following the asymptotic (truncated Taylor-series) expansions (A 1), the velocity components in the vicinity of the wall are expanded as (Mansour *et al.* 1988)

$$u'^+ \underset{y^+ \rightarrow 0}{\sim} A_u^+(x^+, z^+, t^+) y^+ + B_u^+(x^+, z^+, t^+) y^{+2} + C_u^+(x^+, z^+, t^+) y^{+3} + \dots \quad (2.3a)$$

$$v'^+ \underset{y^+ \rightarrow 0}{\sim} B_v^+(x^+, z^+, t^+) y^{+2} + C_v^+(x^+, z^+, t^+) y^{+3} + \dots \quad (2.3b)$$

$$w'^+ \underset{y^+ \rightarrow 0}{\sim} A_w^+(x^+, z^+, t^+) y^+ + B_w^+(x^+, z^+, t^+) y^{+2} + C_w^+(x^+, z^+, t^+) y^{+3} + \dots \quad (2.3c)$$

to satisfy the no-slip condition $u'_i(x, y^+ = 0, z, t) = 0$ at the wall (A 2), and the fluctuating continuity equation (3.2a), whose limit at the wall is $\lim_{y^+ \rightarrow 0} (\partial_{y^+} v'^+) = 0 \xrightarrow{(A1)} A_v^+ = 0$, i.e. $v'^+ \propto y^{+2}$ as $y^+ \rightarrow 0$ (2.3b). Expansions (2.3) of the near-wall fluctuating-velocity field are valid for general 3-D xyz -inhomogeneous turbulent incompressible flow near a plane no-slip wall. Assuming (2.3), straightforward calculations yield the asymptotic expansions of r_{ij}^+ and ε_{ij}^+ , from which (§A.2) are calculated the asymptotic expansions of b_{ij} (Tab. 1), $b_{\varepsilon_{ij}}$ (Tab. 2), and of their invariants (Tabs. 1, 2). Obviously (Tabs. 1, 2) the wall-values of the anisotropy tensors b_{ij} and $b_{\varepsilon_{ij}}$ are identical, and their wall-normal gradients are proportional with factor 2, *viz*

$$b_{\varepsilon_{ij}} \underset{y^+ \rightarrow 0}{\sim} (b_{ij})_w + 2 \left(\frac{\partial b_{ij}}{\partial y^+} \right)_w y^+ + O(y^{+2}) \quad (2.4a)$$

with fundamental differences occuring in the $O(y^{+2})$ -terms, those of $b_{\varepsilon_{ij}}$ containing the spatial gradients $(\nabla A'_u)^+$ and $(\nabla A'_w)^+$, contrary to those of b_{ij} . Concerning the wall-normal diagonal components, b_{yy} and $b_{\varepsilon_{yy}}$, whose linear $O(y^+)$ terms are = 0, notice that (Tabs. 1, 2) the wall-normal 2-derivatives are proportional with a factor 4

$$b_{\varepsilon_{yy}} \underset{y^+ \rightarrow 0}{\sim} (b_{yy})_w + 4 \left(\frac{1}{2} \frac{\partial^2 b_{yy}}{\partial y^{+2}} \right)_w y^{+2} + O(y^{+3}) \quad (2.4b)$$

Relation (2.4a) carries over (Tabs. 1, 2) to the anisotropy invariants (2.1b, 2.2b)

$$\Pi_{\mathbf{b}_\varepsilon} \underset{y^+ \rightarrow 0}{\sim} (\Pi_{\mathbf{b}})_w + 2 \left(\frac{\partial \Pi_{\mathbf{b}}}{\partial y^+} \right)_w y^+ + O(y^{+2}) \quad (2.4c)$$

$$\text{III}_{\mathbf{b}_\varepsilon} \underset{y^+ \rightarrow 0}{\sim} (\text{III}_{\mathbf{b}})_w + 2 \left(\frac{\partial \text{III}_{\mathbf{b}}}{\partial y^+} \right)_w y^+ + O(y^{+2}) \quad (2.4d)$$

$$\begin{aligned}
b_{xx} &\sim \frac{2\overline{A_u'^{+2}} - \overline{A_w'^{+2}}}{3\left(\overline{A_u'^{+2}} + \overline{A_w'^{+2}}\right)} + \frac{2\overline{A_u'^{+2}}\overline{A_u'^{+2}}B_u'^{+2} - \overline{A_u'^{+2}}\overline{A_w'^{+2}}\overline{A_w'^{+2}}B_w'^{+2}}{\left(\overline{A_u'^{+2}} + \overline{A_w'^{+2}}\right)^2} y^+ + O(y^{+2}) \\
b_{xy} &\sim \frac{\overline{A_u'^{+2}}B_u'^{+2}}{\overline{A_u'^{+2}} + \overline{A_w'^{+2}}} y^+ + O(y^{+2}) \\
b_{yy} &\sim -\frac{1}{3} + \frac{\overline{B_v'^{+2}}}{\overline{A_u'^{+2}} + \overline{A_w'^{+2}}} y^{+2} + O(y^{+3}) \\
b_{yz} &\sim \left[\frac{\overline{A_u'^{+2}}B_u'^{+2}}{\overline{A_u'^{+2}} + \overline{A_w'^{+2}}} y^+ + O(y^{+2}) \right] \\
b_{zz} &\sim \frac{\overline{A_w'^{+2}} - \overline{A_u'^{+2}}}{3\left(\overline{A_u'^{+2}} + \overline{A_w'^{+2}}\right)} - 2\frac{\overline{A_u'^{+2}}\overline{A_u'^{+2}}B_u'^{+2} - \overline{A_u'^{+2}}\overline{A_w'^{+2}}\overline{A_w'^{+2}}B_w'^{+2}}{\left(\overline{A_u'^{+2}} + \overline{A_w'^{+2}}\right)^2} y^+ + O(y^{+2}) \\
b_{zx} &\sim \left[\frac{\overline{A_u'^{+2}}\overline{A_w'^{+2}}}{\overline{A_u'^{+2}} + \overline{A_w'^{+2}}} + \frac{\left(\overline{A_u'^{+2}} + \overline{A_w'^{+2}}\right)\left(\overline{A_u'^{+2}}B_u'^{+2} + \overline{A_w'^{+2}}B_w'^{+2}\right)}{\left(\overline{A_u'^{+2}} + \overline{A_w'^{+2}}\right)^2} y^+ + O(y^{+2}) \right] \\
\Pi_b &\sim -\frac{\overline{A_u'^{+2}2^2} - \overline{A_u'^{+2}}\overline{A_w'^{+2}} + \overline{A_w'^{+2}2^2} + \left[3\overline{A_u'^{+2}}\overline{A_w'^{+2}} \right]}{3\left(\overline{A_u'^{+2}} + \overline{A_w'^{+2}}\right)^2} + \left(\frac{\left(\overline{A_u'^{+2}} - \overline{A_u'^{+2}}\overline{A_w'^{+2}}\right)\overline{A_w'^{+2}}B_w'^{+2} + \left(\overline{A_u'^{+2}} - \overline{A_u'^{+2}}\overline{A_w'^{+2}}\right)\overline{A_u'^{+2}}B_u'^{+2}}{\left(\overline{A_u'^{+2}} + \overline{A_w'^{+2}}\right)^3} \right. \\
&\quad \left. + \left[\frac{4\overline{A_u'^{+2}}\overline{A_w'^{+2}}\left(\overline{A_u'^{+2}}B_u'^{+2} + \overline{A_w'^{+2}}B_w'^{+2}\right) - 2\overline{A_u'^{+2}}\overline{A_u'^{+2}}\left(\overline{A_u'^{+2}} + \overline{A_w'^{+2}}\right)\left(\overline{A_u'^{+2}}B_w'^{+2} + \overline{A_w'^{+2}}B_u'^{+2}\right)}{\left(\overline{A_u'^{+2}} + \overline{A_w'^{+2}}\right)^3} \right] y^+ + O(y^{+2}) \right) \\
\Pi_b &\sim \frac{2\left(\overline{A_u'^{+2}} + \overline{A_w'^{+2}2^2}\right) - 5\overline{A_u'^{+2}}\overline{A_w'^{+2}} + \left[9\overline{A_u'^{+2}}\overline{A_w'^{+2}} \right]}{27\left(\overline{A_u'^{+2}} + \overline{A_w'^{+2}}\right)^2} - \left(\frac{\left(\overline{A_u'^{+2}} - \overline{A_u'^{+2}}\overline{A_w'^{+2}}\right)\overline{A_w'^{+2}}B_w'^{+2} + \left(\overline{A_u'^{+2}} - \overline{A_u'^{+2}}\overline{A_w'^{+2}}\right)\overline{A_u'^{+2}}B_u'^{+2}}{3\left(\overline{A_u'^{+2}} + \overline{A_w'^{+2}}\right)^3} \right. \\
&\quad \left. + \left[\frac{4\overline{A_u'^{+2}}\overline{A_w'^{+2}}\left(\overline{A_u'^{+2}}B_u'^{+2} + \overline{A_w'^{+2}}B_w'^{+2}\right) - 2\overline{A_u'^{+2}}\overline{A_u'^{+2}}\left(\overline{A_u'^{+2}} + \overline{A_w'^{+2}}\right)\left(\overline{A_u'^{+2}}B_w'^{+2} + \overline{A_w'^{+2}}B_u'^{+2}\right)}{3\left(\overline{A_u'^{+2}} + \overline{A_w'^{+2}}\right)^3} \right] y^+ + O(y^{+2}) \right) \\
A &\sim 27\frac{\overline{A_u'^{+2}}\overline{A_w'^{+2}}\overline{B_v'^{+2}} - \overline{A_u'^{+2}}\overline{A_w'^{+2}}\overline{B_v'^{+2}} - \left[\overline{A_u'^{+2}}\overline{A_w'^{+2}}\overline{B_v'^{+2}} + \overline{A_u'^{+2}}\overline{A_w'^{+2}}\overline{B_v'^{+2}} - 2\overline{A_u'^{+2}}\overline{A_u'^{+2}}\overline{A_w'^{+2}}\overline{B_v'^{+2}}\overline{B_v'^{+2}} \right]}{\left(\overline{A_u'^{+2}} + \overline{A_w'^{+2}}\right)^3} y^{+2} + O(y^{+3})
\end{aligned}$$

TABLE 1. Asymptotic (as $y^+ \rightarrow 0$) expansions of \mathbf{b} (2.1a) and of its invariants (2.1b), for general inhomogeneous incompressible (3.2a) turbulent flow near a plane no-slip (A_1, A_2) xz -wall (terms within square brackets $[\dots]$ are 3-D terms which are identically = 0 for 2-D in-the-mean flow).

$$\begin{aligned}
b_{\varepsilon xy} &\sim \frac{\overline{2A_u'^{+2}} - \overline{A_w'^{+2}}}{3\left(\overline{A_u'^{+2}} + \overline{A_w'^{+2}}\right)} + \frac{\overline{A_w'^{+2}} \overline{A_u'^{+2}} B_u'^{+2} - \overline{A_u'^{+2}} \overline{A_w'^{+2}} B_w'^{+2}}{\left(\overline{A_u'^{+2}} + \overline{A_w'^{+2}}\right)^2} y^+ + O(y^{+2}) \\
b_{\varepsilon xy} &\sim \frac{\overline{A_u'^{+2}} B_u'^{+2}}{\overline{A_u'^{+2}} + \overline{A_w'^{+2}}} y^+ + O(y^{+2}) \\
b_{\varepsilon yz} &\sim -\frac{1}{3} + \frac{\overline{B_v'^{+2}}}{\overline{A_u'^{+2}} + \overline{A_w'^{+2}}} y^{+2} + O(y^{+3}) \\
b_{\varepsilon yz} &\sim \left[\frac{\overline{A_u'^{+2}} \overline{B_v'^{+2}}}{\overline{A_u'^{+2}} + \overline{A_w'^{+2}}} y^+ + O(y^{+2}) \right] \\
b_{\varepsilon zz} &\sim \frac{\overline{2A_w'^{+2}} - \overline{A_u'^{+2}}}{3\left(\overline{A_u'^{+2}} + \overline{A_w'^{+2}}\right)} - \frac{\overline{A_w'^{+2}} \overline{A_u'^{+2}} B_u'^{+2} - \overline{A_u'^{+2}} \overline{A_w'^{+2}} B_w'^{+2}}{\left(\overline{A_u'^{+2}} + \overline{A_w'^{+2}}\right)^2} y^+ + O(y^{+2}) \\
b_{\varepsilon zx} &\sim \left[\frac{\overline{A_u'^{+2}} \overline{A_w'^{+2}}}{\overline{A_u'^{+2}} + \overline{A_w'^{+2}}} + 2 \frac{\left(\overline{A_u'^{+2}} + \overline{A_w'^{+2}}\right) \left(\overline{A_u'^{+2}} B_u'^{+2} + \overline{A_w'^{+2}} B_w'^{+2}\right) - 2 \overline{A_u'^{+2}} \overline{A_w'^{+2}} \left(\overline{A_u'^{+2}} B_u'^{+2} + \overline{A_w'^{+2}} B_w'^{+2}\right)}{\left(\overline{A_u'^{+2}} + \overline{A_w'^{+2}}\right)^2} y^+ + O(y^{+2}) \right] \\
\text{II } b_{\varepsilon} &\sim -\frac{\overline{A_u'^{+2}} - \overline{A_u'^{+2}} \overline{A_w'^{+2}} + \overline{A_w'^{+2}}^2}{3\left(\overline{A_u'^{+2}} + \overline{A_w'^{+2}}\right)^2} + \frac{\left[\overline{3A_u'^{+2}} \overline{A_w'^{+2}}\right]}{2} \left(\frac{\left(\overline{A_u'^{+2}} - \overline{A_u'^{+2}} \overline{A_w'^{+2}}\right) \overline{A_u'^{+2}} B_u'^{+2} + \left(\overline{A_w'^{+2}}^2 - \overline{A_u'^{+2}} \overline{A_w'^{+2}}\right) \overline{A_u'^{+2}} B_w'^{+2}}{\left(\overline{A_u'^{+2}} + \overline{A_w'^{+2}}\right)^3} \right. \\
&\quad \left. + \left[\frac{\overline{4A_u'^{+2}} \overline{A_w'^{+2}} \left(\overline{A_u'^{+2}} B_u'^{+2} + \overline{A_w'^{+2}} B_w'^{+2}\right) - 2 \overline{A_u'^{+2}} \overline{A_w'^{+2}} \left(\overline{A_u'^{+2}} + \overline{A_w'^{+2}}\right) \left(\overline{A_u'^{+2}} B_u'^{+2} + \overline{A_w'^{+2}} B_w'^{+2}\right)}{\left(\overline{A_u'^{+2}} + \overline{A_w'^{+2}}\right)^3} \right] y^+ + O(y^{+2}) \right) \\
\text{III } b_{\varepsilon} &\sim \frac{2\left(\overline{A_u'^{+2}} + \overline{A_w'^{+2}}\right) - 5 \overline{A_u'^{+2}} \overline{A_w'^{+2}} + \left[\overline{9A_u'^{+2}} \overline{A_w'^{+2}}\right]}{27\left(\overline{A_u'^{+2}} + \overline{A_w'^{+2}}\right)^2} - 2 \left(\frac{\left(\overline{A_u'^{+2}} - \overline{A_u'^{+2}} \overline{A_w'^{+2}}\right) \overline{A_u'^{+2}} B_u'^{+2} + \left(\overline{A_w'^{+2}}^2 - \overline{A_u'^{+2}} \overline{A_w'^{+2}}\right) \overline{A_u'^{+2}} B_w'^{+2}}{3\left(\overline{A_u'^{+2}} + \overline{A_w'^{+2}}\right)^3} \right. \\
&\quad \left. + \left[\frac{\overline{4A_u'^{+2}} \overline{A_w'^{+2}} \left(\overline{A_u'^{+2}} B_u'^{+2} + \overline{A_w'^{+2}} B_w'^{+2}\right) - 2 \overline{A_u'^{+2}} \overline{A_w'^{+2}} \left(\overline{A_u'^{+2}} + \overline{A_w'^{+2}}\right) \left(\overline{A_u'^{+2}} B_u'^{+2} + \overline{A_w'^{+2}} B_w'^{+2}\right)}{3\left(\overline{A_u'^{+2}} + \overline{A_w'^{+2}}\right)^3} \right] y^+ + O(y^{+2}) \right) \\
A_{\varepsilon} &\sim 108 \frac{\overline{A_u'^{+2}} \overline{A_w'^{+2}} \overline{B_v'^{+2}} - \overline{A_u'^{+2}} \overline{A_w'^{+2}} \overline{B_v'^{+2}} - \left[\overline{A_u'^{+2}} \overline{A_w'^{+2}} \overline{B_v'^{+2}} + \overline{A_u'^{+2}} \overline{A_w'^{+2}} \overline{B_v'^{+2}} - 2 \overline{A_u'^{+2}} \overline{A_w'^{+2}} \overline{A_u'^{+2}} \overline{B_v'^{+2}} \overline{A_w'^{+2}} \overline{B_v'^{+2}}\right]}{\left(\overline{A_u'^{+2}} + \overline{A_w'^{+2}}\right)^3} y^{+2} + O(y^{+3})
\end{aligned}$$

TABLE 2. Asymptotic (as $y^+ \rightarrow 0$) expansions of b_{ε} (2.2*d*) and of its invariants (2.2*b*), for general inhomogeneous incompressible (3.2*d*) turbulent flow near a plane no-slip (A 1, A 2) xz -wall (terms within square brackets [...] are 3-D terms which are identically = 0 for 2-D in-the-mean flow).

Consistent with the 2-C componentality of both r_{ij} (2.1a) and ε_{ij} (2.2a) at the wall (Launder & Shima 1989; Hanjalić 1994; Craft & Launder 2001), the wall-values of the corresponding Lumley's flatness parameters (2.1b, 2.2b) $A_w = (A_\varepsilon)_w = 0$ (Lumley 1978; Simonsen & Krogstad 2005). Furthermore, both A and A_ε tend to 0 quadratically as $y^+ \rightarrow 0$, and their wall-normal 2-derivatives are proportional by a factor 4 (Tabs. 1, 2)

$$A \underset{y^+ \rightarrow 0}{\sim} O(y^{+2}) \quad (2.5a)$$

$$A_\varepsilon \underset{y^+ \rightarrow 0}{\sim} 4 \left(\frac{1}{2} \frac{\partial^2 A}{\partial y^{+2}} \right)_w y^{+2} + O(y^{+3}) \quad (2.5b)$$

because, as can be verified by straightforward calculation, the constant and linear terms in the expansion of the invariants $\{\Pi_{\mathbf{b}}, \text{III}_{\mathbf{b}}, \Pi_{\mathbf{b}_\varepsilon}, \text{III}_{\mathbf{b}_\varepsilon}\}$ (Tabs. 1, 2), cancel out

$$9 (\Pi_{\mathbf{b}})_w + 27 (\text{III}_{\mathbf{b}})_w = 9 (\Pi_{\mathbf{b}_\varepsilon})_w + 27 (\text{III}_{\mathbf{b}_\varepsilon})_w = -1 \quad (2.5c)$$

$$9 \left(\frac{\partial \Pi_{\mathbf{b}}}{\partial y^+} \right)_w + 27 \left(\frac{\partial \text{III}_{\mathbf{b}}}{\partial y^+} \right)_w = 9 \left(\frac{\partial \Pi_{\mathbf{b}_\varepsilon}}{\partial y^+} \right)_w + 27 \left(\frac{\partial \text{III}_{\mathbf{b}_\varepsilon}}{\partial y^+} \right)_w = 0 \quad (2.5d)$$

Of course, calculations retaining the $O(y^{+2})$ -terms in the expansions of the invariants were required to obtain the result (2.5d).

Regarding b_{ij} (Tab. 1), the new results in the paper, with reference to Hanjalić (1994, Tab. 3, p. 191) are the asymptotic expansions of the invariants $\Pi_{\mathbf{b}}$ and $\text{III}_{\mathbf{b}}$, and in particular of the flatness parameter A . Corresponding expansions were obtained (Tab. 2) for $b_{\varepsilon_{ij}}$ and for its invariants $(\Pi_{\mathbf{b}_\varepsilon}, \text{III}_{\mathbf{b}_\varepsilon}, A_\varepsilon)$. With regard to the relations between b_{ij} and $b_{\varepsilon_{ij}}$, Mansour *et al.* (1988, p. 32) have "point(ed) out that close to the wall, Taylor-series expansions of $b_{\varepsilon_{ij}}$ and b_{ij} show that they are equal only up to $O(y^+)$ "; this remark clearly implies $(b_{\varepsilon_{ij}})_w = (b_{ij})_w$. The present results (2.4, 2.5) show the proportionality relation $(\partial_{y^+} b_{ij})_w \stackrel{(2.4a)}{=} \frac{1}{2} (\partial_{y^+} b_{\varepsilon_{ij}})_w$ of the wall-normal gradients and the corresponding relation between the wall-normal gradients of the invariants $(\partial_{y^+} \Pi_{\mathbf{b}_\varepsilon})_w \stackrel{(2.4c)}{=} 2 (\partial_{y^+} \Pi_{\mathbf{b}})_w$ and $(\partial_{y^+} \text{III}_{\mathbf{b}_\varepsilon})_w \stackrel{(2.4d)}{=} 2 (\partial_{y^+} \text{III}_{\mathbf{b}})_w$ on the one hand, and the quadratic asymptotic behaviour of the flatness parameters $A_\varepsilon \underset{y^+ \rightarrow 0}{\sim} 4A + O(y^{+3}) \stackrel{(2.5a)}{\propto}_{y^+ \rightarrow 0} O(y^{+2})$ on the other hand.

2.3. Re_{τ_w} -influence on anisotropy

The evolution of mean-flow and turbulence structure with Re_{τ_w} (A 3g) is central in wall-turbulence research (Marusic *et al.* 2010, 2013; Kim 2012) and DNS of turbulent plane channel flow at progressively higher Re_{τ_w} (Moser *et al.* 1999; Hoyas & Jiménez 2006, 2008; Bernardini *et al.* 2014; Lee & Moser 2015) contribute towards answering several open questions on very-high- Re asymptotics. Turbulence structure is generally represented by nondimensional ratios of turbulent quantities (Bradshaw 1967). In this respect, the anisotropy tensors b_{ij} (2.1a) and $b_{\varepsilon_{ij}}$ (2.2a), and their AIMs (Lumley & Newman 1977; Lumley 1978; Lee & Reynolds 1987; Simonsen & Krogstad 2005) are particularly useful in understanding the differences in behaviour between the Reynolds-stresses r_{ij} (2.1a) and their dissipation-rates ε_{ij} (2.2a), across the channel (in the wall-normal direction y) and with varying Reynolds number Re_{τ_w} (A 3g).

2.3.1. Anisotropy tensors

The strong anisotropy of the Reynolds-stresses in wall-turbulence is related to the anisotropy of the dissipation-rate tensor ε_{ij} (Gerolymos *et al.* 2012b), and it is established that the behaviour of the anisotropy tensor of the Reynolds-stresses b_{ij} differs from

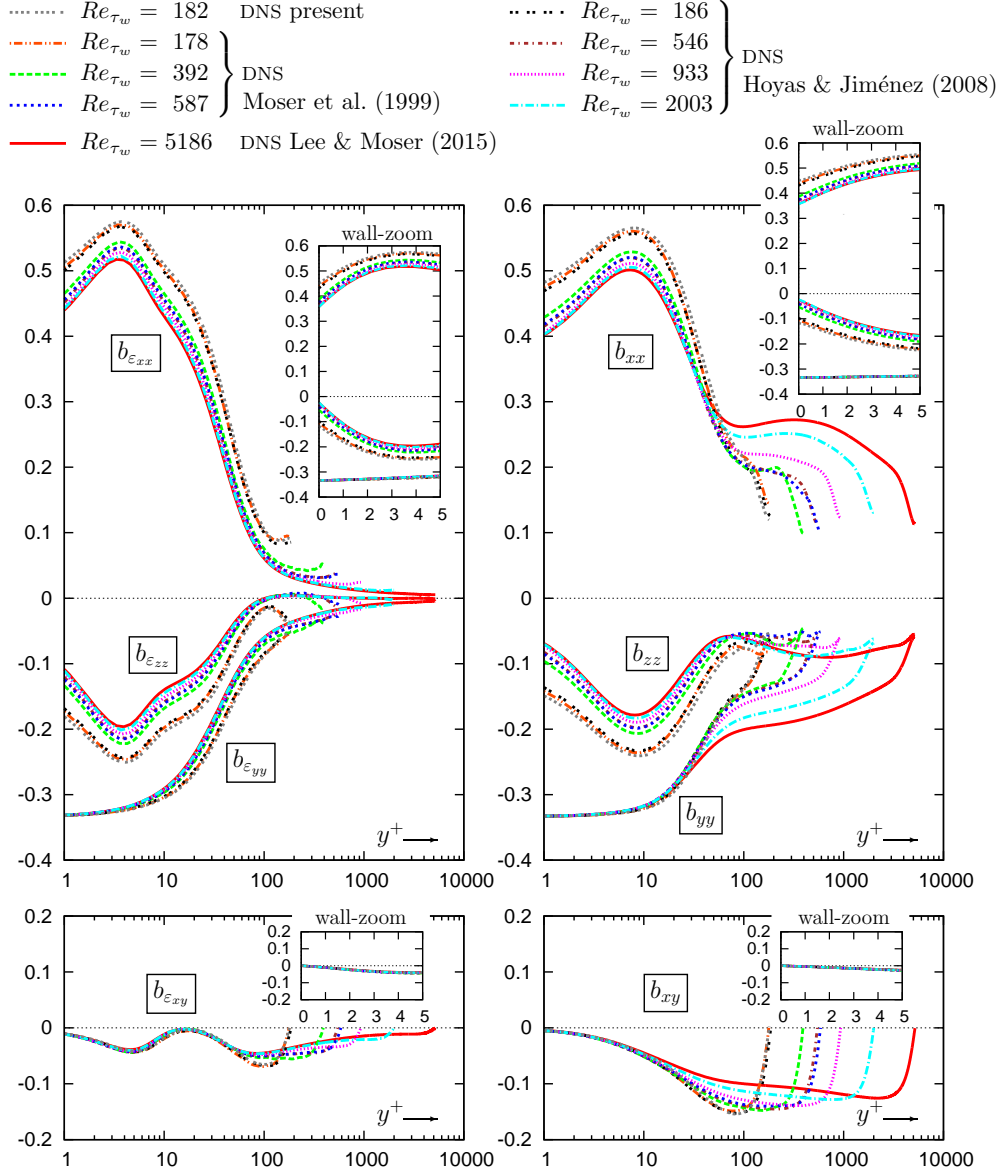


FIGURE 1. Anisotropy (2.1, 2.2) of the normal (b_{xx} , b_{yy} , b_{zz}) and shear (b_{xy}) Reynolds-stresses, and of the corresponding dissipation-rates ($b_{\epsilon_{xx}}$, $b_{\epsilon_{yy}}$, $b_{\epsilon_{zz}}$, $b_{\epsilon_{xy}}$), from existing (Moser *et al.* 1999; del Álamo & Jiménez 2003; Hoyas & Jiménez 2006, 2008; Lee & Moser 2015) DNS computations of turbulent plane channel flow, in the range $Re_{\tau_w} \in [180, 5200]$, plotted against the inner-scaled (A 3c) wall-distance y^+ (logscale and linear wall-zoom).

that of the anisotropy-tensor of the dissipation-rate $b_{\epsilon_{ij}}$ (Launder & Reynolds 1983; Lai & So 1990; Jovanović *et al.* 1995; Jakirlić & Hanjalić 2002). This is obvious by examining (Fig. 1) existing (Moser *et al.* 1999; del Álamo & Jiménez 2003; Hoyas & Jiménez 2006, 2008; Lee & Moser 2015) DNS results which include budgets of r_{ij} -transport (and hence data for the components of ϵ_{ij}), covering the range $Re_{\tau_w} \in [178, 5186]$. Recall that (§2.2), at the wall ($y^+ = 0$), the anisotropy tensors b_{ij} and $b_{\epsilon_{ij}}$ are identical

- Hoyas & Jiménez (2006, 2008); Lozano-Durán & Jiménez (2014)
- △ Moser et al. (1999)
- ◇ Vreman & Kuerten (2014, 2016)
- present
- Bernardini et al. (2014)
- ◇ Hu et al. (2006)
- Lee & Moser (2015)

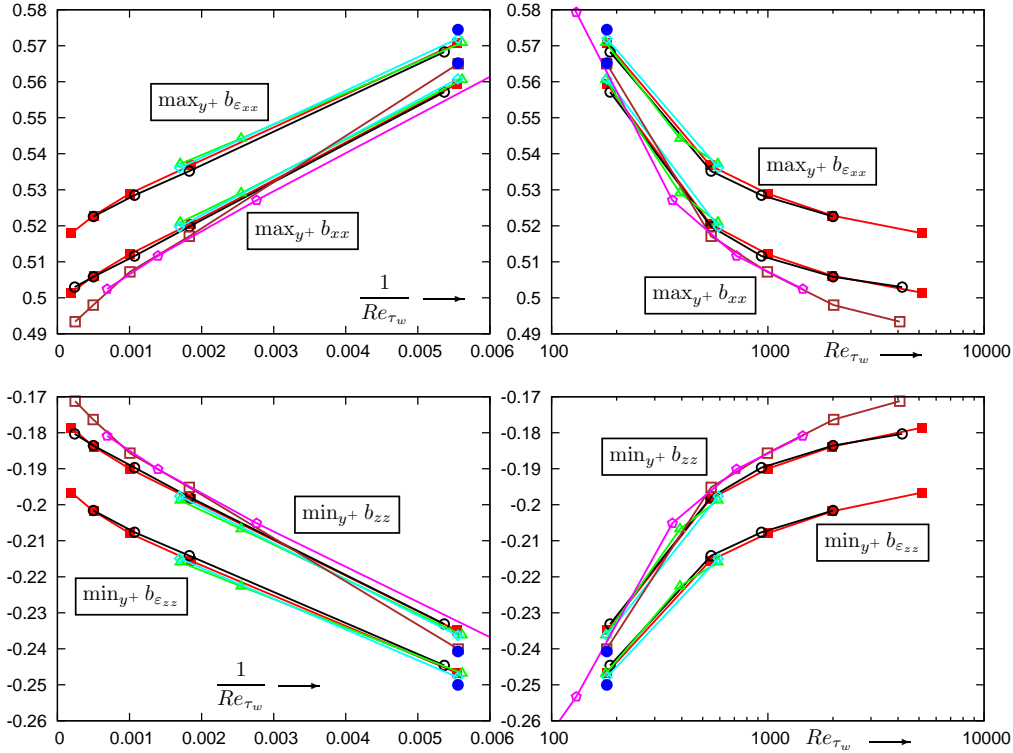


FIGURE 2. Near-wall peaks of the streamwise ($\max_{y^+} b_{xx}$, $\max_{y^+} b_{\varepsilon_{xx}}$) and spanwise ($\min_{y^+} b_{zz}$, $\min_{y^+} b_{\varepsilon_{zz}}$) components of the anisotropy-tensors of the Reynolds-stresses \mathbf{b} (2.1) and of the corresponding dissipation-rates \mathbf{b}_ε (2.2), as a function of the friction Reynolds number ($A3g$) Re_{τ_w} (logscale) and of its inverse $Re_{\tau_w}^{-1}$ (linear scale), from existing (Moser *et al.* 1999; Hu *et al.* 2006; Hoyas & Jiménez 2006, 2008; Lozano-Durán & Jiménez 2014; Bernardini *et al.* 2014; Vreman & Kuerten 2014*b*, 2016; Lee & Moser 2015) DNS computations of turbulent plane channel flow, in the range $Re_{\tau_w} \in [100, 5200]$.

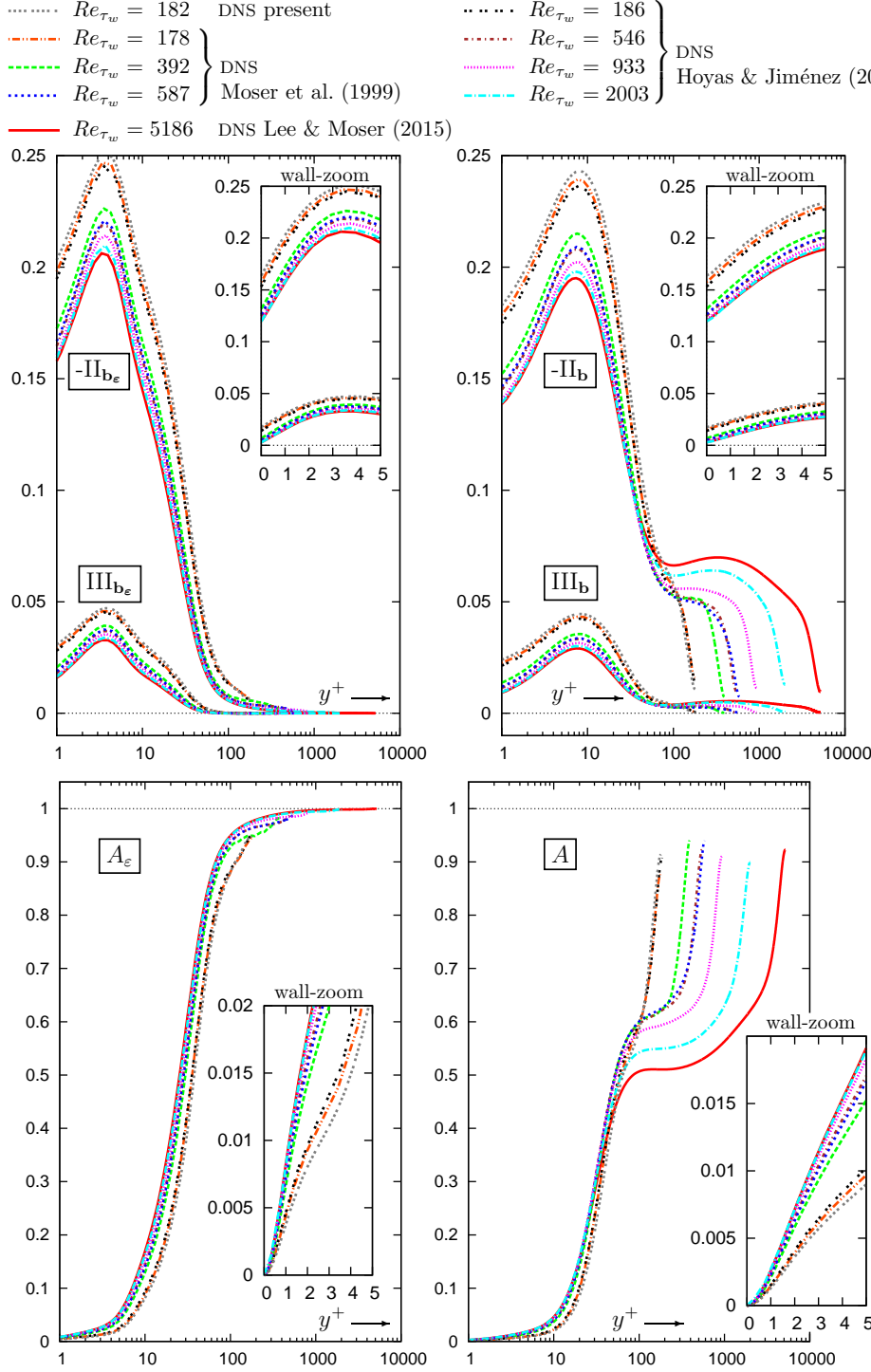
(Mansour *et al.* 1988, p. 32), but the wall-normal gradient of $b_{\varepsilon_{ij}}$ is exactly twice that of b_{ij} (2.4*a*). This explains the near-wall ($y^+ < 10$) evolution of the streamwise (b_{xx} , $b_{\varepsilon_{xx}}$) and spanwise (b_{zz} , $b_{\varepsilon_{zz}}$) components of the anisotropy tensors (Fig. 1), *viz* that $\{b_{\varepsilon_{xx}}, |b_{\varepsilon_{zz}}|\}$ increase much faster with y^+ , and reach their maxima at $y^+ \in [3, 4]$, nearer the wall compared to $\{b_{xx}, |b_{zz}|\}$ which reach their maxima at $y^+ \in [7, 9]$. These near-wall maxima of $\{b_{xx}, |b_{zz}|, b_{\varepsilon_{xx}}, |b_{\varepsilon_{zz}}|\}$ are also global maxima across the channel (Fig. 1). Notice that at fixed Re_{τ_w} the maximum of the spanwise component occurs at slightly higher y^+ than the maximum of the streamwise component, both for b_{ij} and $b_{\varepsilon_{ij}}$ (Fig. 1). Furthermore, at fixed Re_{τ_w} , the values of the maxima are quite close ($\max_y b_{xx} \approx \max_y b_{\varepsilon_{xx}}$ and

$\max_y |b_{zz}| \approx \max_y |b_{\varepsilon_{zz}}|$) but ε_{ij} is slightly more anisotropic than r_{ij} (Fig. 1). In the near-wall region ($y^+ \lesssim 10$), the anisotropy of the streamwise (b_{xx} , $b_{\varepsilon_{xx}}$) and spanwise (b_{zz} , $b_{\varepsilon_{zz}}$) components decreases with increasing Re_{τ_w} , first quite sharply ($Re_{\tau_w} < 400$) and then more slowly (Fig. 1). Careful examination of the values of the maxima *vs* Re_{τ_w} (Fig. 2) suggests that they probably tend to Re_{τ_w} -independent values as Re_{τ_w} increases, although these are not reached yet at the highest available $Re_{\tau_w} \approx 5186$ DNS of Lee & Moser (2015). To alleviate the bias of the computational grid, the values of the extrema were determined by fitting a degree-4 interpolating polynomial $p_I(y^+)$ around the on-grid extremum (2 neighbours on each side) and solving $p'_I(y^+) = 0$ by Newton iteration. This generally had no influence on the value of the maximum, but did smooth out variations of its location. Plots (Fig. 2) of the near-wall peaks of the streamwise ($\max_{y^+} b_{xx}$, $\max_{y^+} b_{\varepsilon_{xx}}$) and spanwise ($\min_{y^+} b_{zz}$, $\min_{y^+} b_{\varepsilon_{zz}}$) components *vs* Re_{τ_w} (logscale) hint that asymptotic limits are approached, and this is further verified by plotting the data against $Re_{\tau_w}^{-1}$ (Fig. 2). More sets of data are available for r_{ij} than for ε_{ij} , and 2 slightly distinct curves appear for the b_{ij} -extrema (Fig. 2), but this only affects the precise value of the asymptotic limits as $Re_{\tau_w}^{-1} \rightarrow 0$ ($\sim 2\%$ scatter for $\max_{y^+} b_{xx}$ and $\sim 5\%$ scatter for $\min_{y^+} b_{zz}$). The anisotropy of the wall-normal component is of course highest at the 2-C wall $(b_{yy})_w = (b_{\varepsilon_{yy}})_w = -\frac{1}{3}$ and then becomes less anisotropic with increasing y^+ (Fig. 1). Obviously, the coefficient $\varepsilon_w^{-1} \overline{B_v'^{+2}}$ (Tabs. 1, 2) of the leading quadratic term in (2.4b) slightly increases with increasing Re_{τ_w} (Fig. 1). Finally, regarding the shear components, both b_{xy} and $b_{\varepsilon_{xy}}$ seem Re_{τ_w} -independent near the wall ($y^+ \lesssim 10$).

In contrast to the near-wall region ($y^+ \lesssim 10$), which is dominated by the wall-asymptotic relations (§2.2), the behaviour of $b_{\varepsilon_{ij}}$ is completely different from that of b_{ij} at higher y^+ (Fig. 1). The anisotropy of the streamwise Reynolds-stress component b_{xx} forms, with increasing Re_{τ_w} , a plateau corresponding to the log-region of the mean-velocity profile (Coles 1956) followed by a sharp decrease in the wake-region. The level of anisotropy b_{xx} in the log-region increases with Re_{τ_w} but may be reaching an asymptotic limit, although simulations at higher Re_{τ_w} are needed to ascertain this point. The spanwise component b_{zz} becomes more isotropic with increasing y^+ in the buffer layer ($y^+ \in [10, 100]$), followed by a slight increase in anisotropy in the log-region (Fig. 1), while the wall-normal component b_{yy} becomes more isotropic with increasing y^+ , quite sharply in the buffer-layer and more progressively in the log-region. Interestingly, both b_{yy} and b_{zz} also seem to be forming a log-region plateau with increasing Re_{τ_w} , but simulations at higher Re_{τ_w} are required to verify this trend. Both components b_{yy} and b_{zz} become more anisotropic in the log-region with increasing Re_{τ_w} (Fig. 1). Finally, in the wake-region, both b_{yy} and b_{zz} tend quite sharply to a common centerline value (Fig. 1).

Contrary to b_{ij} , the diagonal components of $b_{\varepsilon_{ij}}$ tend quasi-monotonically to a near-isotropic (but not exactly isotropic) state at the centerline, first steeply in the buffer-layer and then more gradually in the log-region (Fig. 1). The low- Re_{τ_w} data exhibit a clear albeit slight increase in the anisotropy of $\{b_{\varepsilon_{xx}}, b_{\varepsilon_{yy}}, b_{\varepsilon_{zz}}\}$ near the centerline which becomes less pronounced with increasing Re_{τ_w} . Unlike b_{zz} , $b_{\varepsilon_{zz}}$ reaches a near-0 value in the log-region (Fig. 1).

The shear components also behave very differently. The Reynolds-stress anisotropy b_{xy} becomes more anisotropic from the wall up to the beginning of the wake-region, before sharply going to 0 (exactly, because of the symmetry condition $\overline{u'v'}|_{CL} = 0$) at the centerline. The shear component $b_{\varepsilon_{xy}}$ is practically Re_{τ_w} -independent up to the end of the buffer-layer ($y^+ \lesssim 100$), with a wavy shape reaching 0 near $y^+ \approx 20$ (Fig. 1), then being relatively flat in the log-region.



2.3.2. Anisotropy invariants

More precise information on the influence of Re_{τ_w} (A 3g) on the anisotropy of r_{ij} and ε_{ij} can be obtained by considering the invariants $\{\text{III}_{\mathbf{b}}, -\text{II}_{\mathbf{b}}\}$ (2.1b) and $\{\text{III}_{\mathbf{b}_\varepsilon}, -\text{II}_{\mathbf{b}_\varepsilon}\}$ (2.2b) whose locus lies inside Lumley's (1978) realizability triangle (Mansour *et al.* 1988, Figs. 17 and 18, p. 32). As the intervals of possible values (Lumley 1978; Simonsen & Krogstad 2005)

$$\text{II}_{\mathbf{b}} \in \left[-\frac{1}{3}, 0 \right] \ni \text{II}_{\mathbf{b}_\varepsilon} \quad (2.6a)$$

$$\text{III}_{\mathbf{b}} \in \left[-\frac{1}{108}, \frac{2}{27} \right] \ni \text{III}_{\mathbf{b}_\varepsilon} \quad (2.6b)$$

$$A \in [0, 1] \ni A_\varepsilon \quad (2.6c)$$

are rather limited, the invariants are quite sensitive indicators of anisotropy, and this sensitivity is visible in the influence of Re_{τ_w} on the near-wall peaks of the invariants (Fig. 3). The evolution of the invariants with y^+ and Re_{τ_w} (Fig. 3) is very similar to what was observed for the diagonal components of the anisotropy tensors (Fig. 1). Near the wall, $\{\text{III}_{\mathbf{b}_\varepsilon}, -\text{II}_{\mathbf{b}_\varepsilon}\}$ increase faster with y^+ compared to $\{\text{III}_{\mathbf{b}}, -\text{II}_{\mathbf{b}}\}$, in line with (2.4c, 2.4d), reaching their maxima at $y^+ \in [3, 4]$ compared to $y^+ \in [7, 9]$ (Fig. 3), ε_{ij} being slightly more anisotropic than r_{ij} . Near the wall, A_ε increases much faster with y^+ compared to A (Fig. 3), in line with (2.5a, 2.5b). There is noticeable Re_{τ_w} -influence for $Re_{\tau_w} < 400$ both in wall values and in rate-of-increase with y^+ for all of the invariants (Fig. 3). On the other hand, with increasing Re_{τ_w} , it would seem that an asymptotic state is approached in the near-wall region, including the buffer-layer ($y^+ \lesssim 100$), although DNS at higher Re_{τ_w} are still required to fully substantiate this observation. Regarding the invariants of r_{ij} , $\{-\text{II}_{\mathbf{b}}, \text{III}_{\mathbf{b}}, A\}$, a plateau appears with increasing Re_{τ_w} (Fig. 3), marking the log-region of the mean-velocity profile (Lee & Moser 2015), but again DNS at higher Re_{τ_w} are needed to determine whether a Re_{τ_w} -asymptotic value of the level of this plateau exists. On the contrary, the invariants of ε_{ij} $\{-\text{II}_{\mathbf{b}_\varepsilon}, \text{III}_{\mathbf{b}_\varepsilon}, A_\varepsilon\}$ vary monotonically from the wall to centerline, and seem to approach Re_{τ_w} -independent y^+ -distributions with increasing Re_{τ_w} .

2.3.3. AIM at the wall and at the centerline

The variation with Re_{τ_w} of the y^+ -distributions of r_{ij} and ε_{ij} anisotropy (Figs. 1–3) indicates trends in the evolution of turbulence structure with increasing Re_{τ_w} . These trends are better quantified by studying the evolution with Re_{τ_w} of the anisotropy invariants $(-\text{II}_{\mathbf{b}}, \text{III}_{\mathbf{b}}, -\text{II}_{\mathbf{b}_\varepsilon}, \text{III}_{\mathbf{b}_\varepsilon})$ at the wall and at the centerline (Fig. 4). Several of the available DNS data (Kim *et al.* 1987; Moser *et al.* 1999; Hu *et al.* 2002, 2003, 2006; del Álamo & Jiménez 2003; Hoyas & Jiménez 2006, 2008; Lozano-Durán & Jiménez 2014; Bernardini *et al.* 2014; Vreman & Kuerten 2014a,b, 2016; Lee & Moser 2015) acquired since the pioneering work of Kim *et al.* (1987) were considered in this study. These data were obtained by several authors with different computational accuracy indicators (spatio-temporal resolution, box size, observation time and sampling frequency) using a variety of computational methods and/or codes. Notice that for the low $Re_{\tau_w} \approx 180$ case, Vreman & Kuerten (2014a) recently reported a detailed study demonstrating consistent convergence of DNS results with increasing computational accuracy. At the centerline, only databases including ε_{ij} -data (Moser *et al.* 1999; del Álamo & Jiménez 2003; Hoyas & Jiménez 2006, 2008; Vreman & Kuerten 2014b, 2016), were used for the \mathbf{b}_ε -invariants (Fig. 4), and wall-values for the \mathbf{b}_ε -invariants were used when available (Moser *et al.* 1999; del Álamo & Jiménez 2003; Hoyas & Jiménez 2006, 2008). For those databases that did not include wall-values (Vreman & Kuerten 2014b, 2016) or ε_{ij} -data (Hu *et al.* 2006; Bernardini *et al.* 2014; Lozano-Durán & Jiménez 2014) wall-invariants were estimated

by linear extrapolation of the \mathbf{b} -invariants from the first 2 grid-points. The very-near-wall ($y^+ \lesssim 0.2$) data of Bernardini *et al.* (2014) were noisy (presumably because of the extreme near-wall cosine-stretching of the wall-normal mesh-size) and were not used; corresponding wall-values were obtained by extrapolation from the first 2 grid-points with $y^+ \gtrsim 0.2$. The $Re_{\tau_w} \approx 4180$ small-box data of Lozano-Durán & Jiménez (2014) were only used at the wall. Finally, it was found interesting to include the $Re_{\tau_w} < 180$ data of Hu *et al.* (2002, 2003, 2006) illustrating low- Re_{τ_w} asymptotics.

It should be stated from the outset that anisotropy invariants are much more sensitive to r_{ij} and ε_{ij} data uncertainties (Schultz & Flack 2013, p. 5) because of the cumulative propagation of these uncertainties (Taylor 1997, §3, pp. 45–91) in the calculation of the anisotropy tensors (2.1a, 2.2a), and then of their invariants (2.1a, 2.2a). Nonetheless, although data for some of the invariants exhibit substantial scatter (Fig. 4), it appears that Re_{τ_w} -trends can be deduced with reasonable confidence.

At the wall, the data for both $\Pi_{\mathbf{b}_w} \stackrel{(2.4c)}{=} \Pi_{\mathbf{b}_\varepsilon w}$ and $\text{III}_{\mathbf{b}_w} \stackrel{(2.4d)}{=} \text{III}_{\mathbf{b}_\varepsilon w}$ show consistent behaviour with reasonably small scatter (Fig. 4) suggesting that the near-wall DNS data are quite robust with respect to the variation of computational accuracy indicators of the simulations. It seems likely that, with increasing Re_{τ_w} , the wall-invariants reach asymptotic values. On the other hand, as Re_{τ_w} decreases, both invariants increase sharply (Fig. 4). Notice that the very-small-box $Re_{\tau_w} \approx 4180$ data of Lozano-Durán & Jiménez (2014), which were only considered at the wall, are consistent with the large-box data (Bernardini *et al.* 2014; Lee & Moser 2015) suggesting that the small-box bias mainly impacts the centerline region, whereas the very-near-wall behaviour is less sensitive to the details of the large-scale outer-flow structures.

At the centerline, the data show considerable scatter (Fig. 4), especially for the \mathbf{b} -invariants $(-\Pi_{\mathbf{b}}, \text{III}_{\mathbf{b}})_{\text{CL}}$, in line with the observation on the cumulative impact of r_{ij} and ε_{ij} uncertainties on the calculation of the invariants. Notice first that the scatter is more important for the \mathbf{b} -invariants which characterize (Lee & Reynolds 1987) the large-scale anisotropy and are therefore more sensitive to box-size and observation-time, whereas the \mathbf{b}_ε -invariants $(-\Pi_{\mathbf{b}_\varepsilon}, \text{III}_{\mathbf{b}_\varepsilon})_{\text{CL}}$ which characterize the small-scales anisotropy are more robust. With respect to box-size, notice that high- Re_{τ_w} small-box calculations (Lozano-Durán & Jiménez 2014) overpredict the \mathbf{b} -invariants at the centerline by a factor 2 (not included in Fig. 4). This is not completely unexpected, and, in view of the consistent wall-invariants obtained in these high- Re_{τ_w} small-box calculations, it suggests that the very-large-scale structures influence quite substantially turbulence at the centerline and much less in the very-near-wall (sublayer) region. The general trend of the \mathbf{b} -invariants $(-\Pi_{\mathbf{b}}, \text{III}_{\mathbf{b}})_{\text{CL}}$ at the centerline (Fig. 4), is a strong decrease with increasing Re_{τ_w} in the range $Re_{\tau_w} < 400$, followed by a slight increase, probably reaching an asymptotic state with increasing Re_{τ_w} . Nonetheless there is too much scatter in the data to draw definitive conclusions (Fig. 4). Regarding the \mathbf{b}_ε -invariants $(-\Pi_{\mathbf{b}_\varepsilon}, \text{III}_{\mathbf{b}_\varepsilon})_{\text{CL}}$ at the centerline, there appears a clear trend of asymptotic decrease to ≈ 0 as Re_{τ_w} increases (Fig. 4).

Observation of b_{ij} at the centerline (Fig. 1), where by symmetry $b_{xy_{\text{CL}}} = 0$, shows that $b_{yy_{\text{CL}}} \approx b_{zz_{\text{CL}}} < b_{xx_{\text{CL}}}$ (Fig. 1), at least for $Re_{\tau_w} \geq 180$, implying that the Reynolds-stress tensor at the centerline is axisymmetric rod-like (Simonsen & Krogstad 2005, Fig. 4, p. 3). However, the componentality of ε_{ij} at the centerline is not as obvious (Fig. 1), especially as the \mathbf{b}_ε -invariants approach 0 at the centerline (Fig. 4), contrary to the \mathbf{b} -invariants which seem to reach finite asymptotic values at the centerline (Fig. 4). At the rod-like axisymmetric boundary of the realizability triangle (Fig. 4) $\Pi + 3(\frac{1}{4}\text{III}^2)^3 = 0$, so that $\Pi^{-1}(\Pi + 3(\frac{1}{4}\text{III}^2)^3)$ is a diagnostic function whose distance from 0 denotes departure

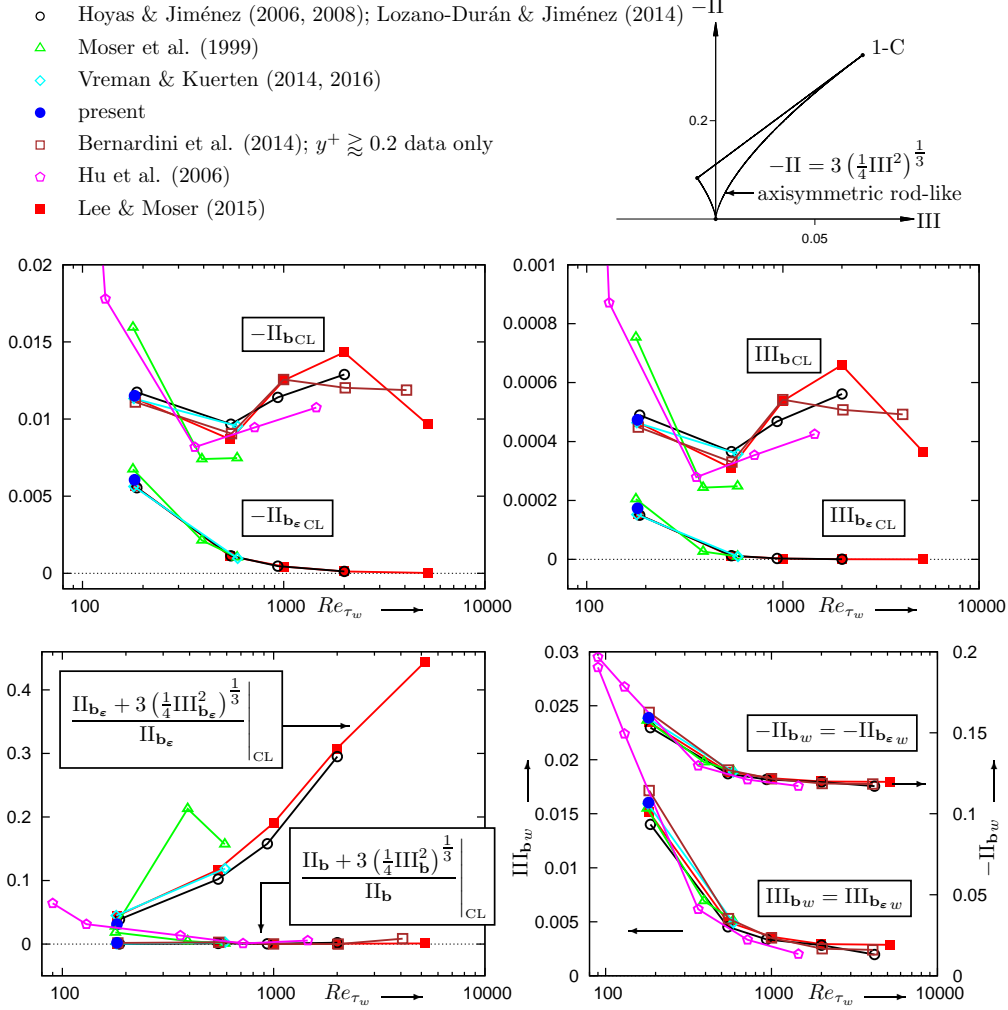


FIGURE 4. Invariants of the anisotropy-tensors (2.1, 2.2) of the Reynolds-stresses \mathbf{b} ($\Pi_{\mathbf{b}}$, $\text{III}_{\mathbf{b}}$) and of the corresponding dissipation-rates \mathbf{b}_{ϵ} ($\Pi_{\mathbf{b}_{\epsilon}}$, $\text{III}_{\mathbf{b}_{\epsilon}}$), at the wall $(\cdot)_w$ and at channel centerline $(\cdot)_{\text{CL}}$, and axisymmetry-diagnostic $\Pi_{\mathbf{b}}^{-1} \left(\Pi_{\mathbf{b}} + 3 \left(\frac{1}{4} \text{III}_{\mathbf{b}}^2 \right)^{\frac{1}{3}} \right)$ and $\Pi_{\mathbf{b}_{\epsilon}}^{-1} \left(\Pi_{\mathbf{b}_{\epsilon}} + 3 \left(\frac{1}{4} \text{III}_{\mathbf{b}_{\epsilon}}^2 \right)^{\frac{1}{3}} \right)$, at the centerline $(\cdot)_{\text{CL}}$, as a function of the friction Reynolds number Re_{τ_w} (A 3g), from existing (Moser *et al.* 1999; Hu *et al.* 2006; Hoyas & Jiménez 2006, 2008; Lozano-Durán & Jiménez 2014; Bernardini *et al.* 2014; Vreman & Kuerten 2014b, 2016; Lee & Moser 2015) DNS computations of turbulent plane channel flow, in the range $Re_{\tau_w} \in [80, 5200]$.

from rod-like axisymmetric componentality. Contrary to \mathbf{b}_{CL} , $\mathbf{b}_{\epsilon \text{CL}}$ at the centerline seems to become increasingly nonaxisymmetric as Re_{τ_w} increases (Fig. 4). Finally, the data of Hu *et al.* (2006) at very-low $Re_{\tau_w} < 180$ seem to indicate departure from rod-like axisymmetry for \mathbf{b}_{CL} (Fig. 4). At $Re_{\tau_w} \approx 180$, the data of Kim *et al.* (1987) also indicate a slight departure from rod-like axisymmetry of \mathbf{b}_{CL} , but all other data (Vreman & Kuerten 2016; Hoyas & Jiménez 2006; Bernardini *et al.* 2014; Lee & Moser 2015), including the present calculations, indicate that \mathbf{b}_{CL} is rod-like axisymmetric at $Re_{\tau_w} \approx 180$ (Fig. 4). Further DNS at very-low $Re_{\tau_w} < 180$ are therefore needed to verify the departure from rod-like axisymmetry of \mathbf{b}_{CL} with decreasing Re_{τ_w} .

3. ε_{ij} -budgets

The dynamics of ε_{ij} are described by an exact transport equation that can be readily obtained by the fluctuating flow equations (§3.1). The budgets of the various terms in the transport equations for ε_{ij} (3.3) are studied for low-Reynolds-number plane channel flow (§3.2).

Notice first that ε_{ij} (1.2a) is generated from the 4-order tensor

$$\mathcal{E}_{ijk m} := 2\nu \overline{\frac{\partial u'_i}{\partial x_k} \frac{\partial u'_j}{\partial x_m}} \xrightarrow{(1.2a)} \varepsilon_{ij} = \mathcal{E}_{ijk m} \delta_{km} = \mathcal{E}_{ijk k} \quad (3.1a)$$

by contraction of the last 2 indices. Considering $\mathcal{E}_{ijk m}$ is important because this 4-order tensor appears in the production mechanisms of ε_{ij} (3.3). The tensor $\mathcal{E}_{ijk m}$ was used by other authors (Durbin & Speziale 1991; Speziale & Gatski 1997) who studied ε_{ij} -transport in homogeneous turbulence. It is also interesting to note that the 9 transport equations for the variances of the fluctuating velocity-gradients studied by Vreman & Kuerten (2014b, (7, 9), p. 4) are also included in the transport equations for $\mathcal{E}_{ijk m}$ (3.1a) because

$$2\nu \overline{\left(\frac{\partial u'_i}{\partial x_j}\right)^2} \in \left\{ \mathcal{E}_{xxxx}, \mathcal{E}_{xxyy}, \mathcal{E}_{xxzz}, \mathcal{E}_{yyxx}, \mathcal{E}_{yyyy}, \mathcal{E}_{yyzz}, \mathcal{E}_{zzxx}, \mathcal{E}_{zzyy}, \mathcal{E}_{zzzz} \right\} \quad (3.1b)$$

3.1. ε_{ij} -transport equation

Starting from the fluctuating continuity (Mathieu & Scott 2000, (4.6), p. 76)

$$\frac{\partial u'_\ell}{\partial x_\ell} = 0 \quad (3.2a)$$

and fluctuating momentum (Mathieu & Scott 2000, (4.31), p. 85)

$$\rho \frac{\partial u'_i}{\partial t} + \rho \bar{u}_\ell \frac{\partial u'_i}{\partial x_\ell} = -\rho \frac{\partial}{\partial x_\ell} \left(u'_i u'_\ell - \overline{u'_i u'_\ell} \right) - \rho u'_\ell \frac{\partial \bar{u}_i}{\partial x_\ell} - \frac{\partial p'}{\partial x_i} + \mu \frac{\partial^2 u'_i}{\partial x_\ell \partial x_\ell} \quad (3.2b)$$

equations we can work out the transport equations for $\mathcal{E}_{ijk m}$ (3.1a), and by contraction (3.1a) the transport equation for ε_{ij} , which reads

$$\begin{aligned} & \underbrace{\rho \frac{\partial \varepsilon_{ij}}{\partial t} + \rho \bar{u}_\ell \frac{\partial \varepsilon_{ij}}{\partial x_\ell}}_{C_{\varepsilon_{ij}}} = \underbrace{\frac{\partial}{\partial x_\ell} \left[\mu \frac{\partial \varepsilon_{ij}}{\partial x_\ell} \right]}_{d_{\varepsilon_{ij}}^{(\mu)}} + \underbrace{\frac{\partial}{\partial x_\ell} \left[-\rho \left(\overline{u'_\ell 2\nu \frac{\partial u'_i}{\partial x_k} \frac{\partial u'_j}{\partial x_k}} \right) \right]}_{d_{\varepsilon_{ij}}^{(u)}} \\ & \underbrace{-\rho \varepsilon_{i\ell} \frac{\partial \bar{u}_j}{\partial x_\ell} - \rho \varepsilon_{j\ell} \frac{\partial \bar{u}_i}{\partial x_\ell}}_{P_{\varepsilon_{ij}}^{(1)}} - \underbrace{\rho \left(2\nu \overline{\frac{\partial u'_i}{\partial x_k} \frac{\partial u'_j}{\partial x_\ell}} \right) \left(\frac{\partial \bar{u}_k}{\partial x_\ell} + \frac{\partial \bar{u}_\ell}{\partial x_k} \right)}_{P_{\varepsilon_{ij}}^{(2)}} \\ & \underbrace{-\rho \left(2\nu \overline{u'_\ell \frac{\partial u'_i}{\partial x_k}} \right) \frac{\partial^2 \bar{u}_j}{\partial x_\ell \partial x_k} - \rho \left(2\nu \overline{u'_\ell \frac{\partial u'_j}{\partial x_k}} \right) \frac{\partial^2 \bar{u}_i}{\partial x_\ell \partial x_k}}_{P_{\varepsilon_{ij}}^{(3)}} - \underbrace{\rho \left[2\nu \frac{\partial u'_\ell}{\partial x_k} \left(\frac{\partial u'_i}{\partial x_k} \frac{\partial u'_j}{\partial x_\ell} + \frac{\partial u'_j}{\partial x_k} \frac{\partial u'_i}{\partial x_\ell} \right) \right]}_{\Xi_{\varepsilon_{ij}} =: P_{\varepsilon_{ij}}^{(4)}} \\ & \underbrace{-2\nu \overline{\frac{\partial u'_i}{\partial x_k} \frac{\partial^2 p'}{\partial x_j \partial x_k}} - 2\nu \overline{\frac{\partial u'_j}{\partial x_k} \frac{\partial^2 p'}{\partial x_i \partial x_k}}}_{\Pi_{\varepsilon_{ij}}} - \underbrace{\rho \left(2\nu \overline{\frac{\partial^2 u'_i}{\partial x_k \partial x_\ell}} \right) \left(2\nu \overline{\frac{\partial^2 u'_j}{\partial x_k \partial x_\ell}} \right)}_{\rho \varepsilon_{\varepsilon_{ij}}} \end{aligned} \quad (3.3)$$

In (3.3) $C_{\varepsilon_{ij}}$ is the convection of ε_{ij} by the mean-flow velocity field \bar{u}_ℓ , $d_{\varepsilon_{ij}}^{(\mu)}$ is the diffusion of ε_{ij} by molecular viscosity (notice that $d_{\varepsilon_{ij}}^{(\mu)} \stackrel{(3.3)}{=} \mu \nabla^2 \varepsilon_{ij}$ for $\mu = \text{const}$), $d_{\varepsilon_{ij}}^{(u)}$ is the turbulent diffusion (mixing) of ε_{ij} by the fluctuating velocity field u'_ℓ , $P_{\varepsilon_{ij}}^{(1)}$ is the production of ε_{ij} by the action of its components on the mean-flow velocity-gradients, $P_{\varepsilon_{ij}}^{(2)}$ is the production of ε_{ij} by the action of $\mathcal{E}_{ijk m}$ (3.1) on the mean-flow velocity-gradients, $P_{\varepsilon_{ij}}^{(3)}$ is the production of ε_{ij} by the mean-flow velocity-Hessian, $P_{\varepsilon_{ij}}^{(4)} := \Xi_{\varepsilon_{ij}}$ corresponds to triple correlations of fluctuating velocity-gradients whose trace $\frac{1}{2}\Xi_{\varepsilon_{\ell\ell}}$ was identified by Mansour *et al.* (1988) as a term "producing" (gain in the budgets of) $\varepsilon := \frac{1}{2}\varepsilon_{\ell\ell}$ (by extension the denomination $P_{\varepsilon_{ij}}^{(4)}$ is used, although this term does not contain gradients of the mean-flow field), $\Pi_{\varepsilon_{ij}}$ are the terms containing the fluctuating pressure-Hessian, and $\varepsilon_{\varepsilon_{ij}}$ is the destruction of ε_{ij} by the action of molecular viscosity. Following usual practice (Mansour *et al.* 1988, (1), p. 17) for the incompressible r_{ij} equations (1.1) and for the ε equation (Mansour *et al.* 1988, (23), p. 23), a computable viscous diffusion term $d_{\varepsilon_{ij}}^{(\mu)}$ was chosen in (3.3), with a corresponding appropriate definition of the destruction-of-dissipation tensor $\varepsilon_{\varepsilon_{ij}}$ (3.3), in lieu of alternative splittings based on the viscous-stress tensor (Ben Nasr *et al.* 2014, (2), p. 189).

Using (3.1) the production of ε_{ij} by mean-flow velocity-gradients reads

$$P_{\varepsilon_{ij}}^{(1)} + P_{\varepsilon_{ij}}^{(2)} \stackrel{(3.3, 3.1a)}{=} \underbrace{-\rho \mathcal{E}_{i\ell k k} \frac{\partial \bar{u}_j}{\partial x_\ell} - \rho \mathcal{E}_{j\ell k k} \frac{\partial \bar{u}_i}{\partial x_\ell}}_{P_{\varepsilon_{ij}}^{(1)}} - \underbrace{\rho \mathcal{E}_{ijk\ell} \left(\frac{\partial \bar{u}_k}{\partial x_\ell} + \frac{\partial \bar{u}_\ell}{\partial x_k} \right)}_{P_{\varepsilon_{ij}}^{(2)}} \quad (3.4)$$

highlighting the importance of considering the generating 4-order tensor $\mathcal{E}_{ijk m}$ (3.1). The separation in 2 terms, $P_{\varepsilon_{ij}}^{(1)}$ and $P_{\varepsilon_{ij}}^{(2)}$, was made to distinguish between the computable (from the knowledge of ε_{ij} and the mean-flow field) term $P_{\varepsilon_{ij}}^{(1)}$, and $P_{\varepsilon_{ij}}^{(2)}$ which involves components of $\mathcal{E}_{ijk m}$ that do not simplify by contraction (3.1a) to ε_{ij} .

3.2. ε_{ij} -transport budgets

Budgets of the ε_{ij} -transport equations (3.3), for turbulent plane channel flow, were obtained (Fig. 5) in an $L_x \times L_y \times L_z = 4\pi\delta \times 2\delta \times \frac{4}{3}\pi\delta$ computational box, using a carefully validated DNS solver (Gerolymos *et al.* 2010, 2013; Gerolymos & Vallet 2014). The resolution in the homogeneous xz -directions is $\Delta x^+ \approx 5.7$ and $\Delta z^+ \approx 1.9$. The wall-normal size of the grid cells adjacent to the wall was $\Delta y_w^+ \approx 0.22$. More importantly, the mesh (65% of the nodes were stretched near the walls geometrically with ratio $r_j = 1.0427$, the remaining nodes in the outer region being equidistant) was kept fine in the entire near-wall region, with $N_{y^+ \leq 10} = 26$ grid cells between the wall and $y^+ \approx 10$, and remained fine up to the centerline where the wall-normal cell-size was $\Delta y_{CL}^+ \approx 3.1$. This spatial resolution, combined with the $O(\Delta\ell^{17})$ scheme used (Gerolymos *et al.* 2009, 2010) is quite fine in view of current state-of-the-art DNS at this $Re_{\tau_w} \approx 180$ (Vreman & Kuerten 2014a, 2016). Statistics were acquired at high sampling frequency (at every iteration; $\Delta t_s^+ = \Delta t^+ \approx 0.0060$, albeit for a relatively short observation time $t_{\text{OBS}}^+ \approx 777$). The close agreement (§4) of the present results for the budgets of the diagonal components with the highly resolved computations of Vreman & Kuerten (2016) further substantiate the validity of the computations. Wall-asymptotics of the various terms in (3.3) can be obtained using the Taylor-expansions (2.3) in the fluctuating-momentum equations (3.2b). Although a full report of these calculations is outside the scope of this paper, some of the limiting wall-values obtained from this procedure are included in the following discussion.

Regarding the streamwise component ε_{xx}^+ (Fig. 5), production $P_{\varepsilon_{xx}}^+$ (gain) roughly bal-

| | | | | | | | | | | | |
|---------------|----------------|-----------------------------|---|--------------|----------------|-------------------|-------------------|--------------|--------------|-------------|----------------|
| Re_{τ_w} | \bar{M}_{CL} | $N_x \times N_y \times N_z$ | $L_x \times L_y \times L_z$ | Δx^+ | Δy_w^+ | $N_{y^+ \leq 10}$ | Δy_{CL}^+ | Δz^+ | Δt^+ | t_{OBS}^+ | Δt_s^+ |
| 182 | 0.35 | $401 \times 201 \times 401$ | $4\pi\delta \times 2\delta \times \frac{4}{3}\pi\delta$ | 5.7 | 0.22 | 26 | 3.1 | 1.9 | 0.0060 | 777 | 0.0060 |

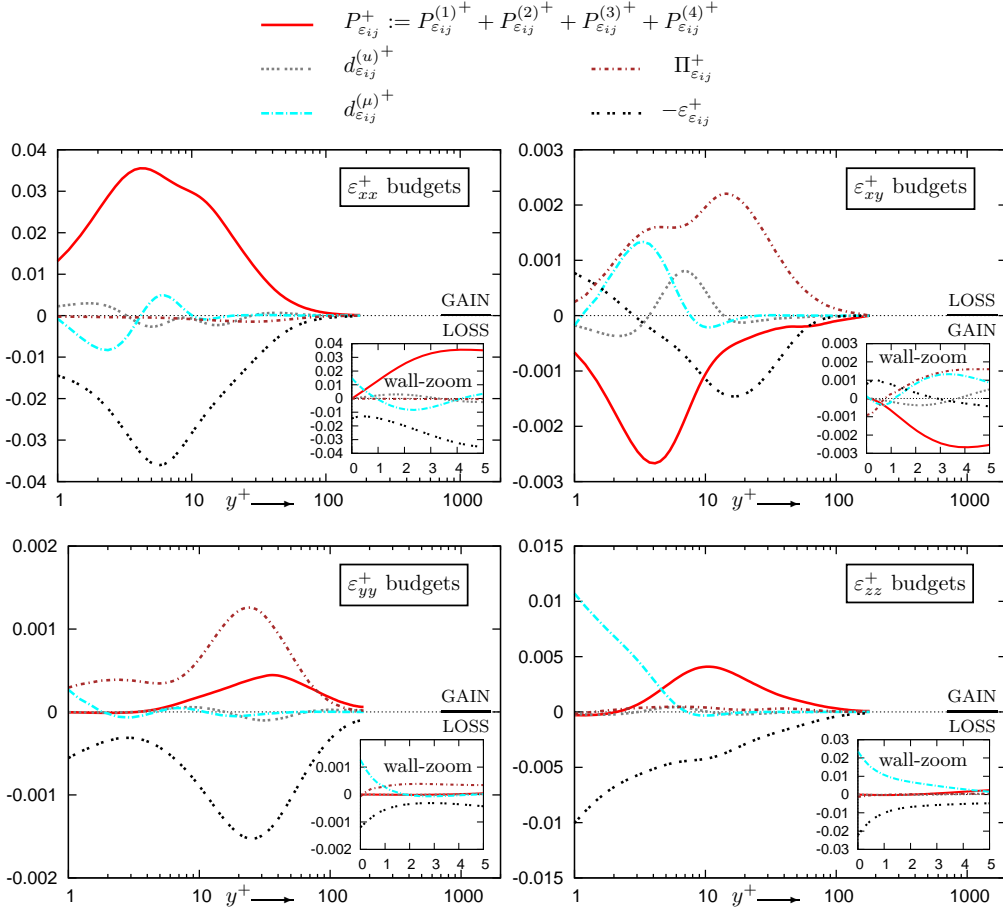


FIGURE 5. Budgets, in wall-units (A 3f), of the transport equations (3.3) for the dissipation tensor ε_{ij} (1.2a), from the present DNS computations of turbulent plane channel flow ($Re_{\tau_w} \approx 182$, $\bar{M}_{CL} \approx 0.35$), plotted against the inner-scaled (A 3c) wall-distance y^+ (logscale and linear wall-zoom).

ances destruction $-\varepsilon_{xx}^+$ (loss) in the major part of the channel ($y^+ \gtrsim 1$), with lesser contributions of diffusion ($d_{xx}^{(u)+} + d_{xx}^{(\mu)+}$). Production P_{xx}^+ peaks at $y^+ \approx 4$ and destruction ε_{xx}^+ at $y^+ \approx 5$. The pressure term Π_{xx}^+ is negligible in the budgets of ε_{xx}^+ throughout the channel. Very near the wall ($y^+ \lesssim 1$; Fig. 5) production $P_{xx}^+ \rightarrow 0$ (wall-asymptotic expansion; §2.2) and viscous diffusion $d_{xx}^{(\mu)+}$ (gain $\forall y^+ \lesssim 1$) roughly counters destruction $-\varepsilon_{xx}^+$ ($y^+ \rightarrow 0$; Fig. 5). At the wall, the pressure term $[\Pi_{xx}^+]_w = 8B'_v \partial_x A'_u \neq 0$ (wall-asymptotic expansion; §2.2). However $[\Pi_{xx}^+]_w \ll [\varepsilon_{xx}^+]_w \approx [d_{xx}^{(\mu)+}]_w$ (Fig. 5).

The budgets of the spanwise component ε_{zz}^+ (Fig. 5) are also dominated by a balance between production P_{zz}^+ (gain) and destruction $-\varepsilon_{zz}^+$ (loss) in the major part of the channel ($y^+ \gtrsim 5$). However, production P_{zz}^+ peaks at $y^+ \approx 10$ and becomes negligible at $y^+ \approx 3$ as $P_{zz}^+ \rightarrow 0$ (wall-asymptotic expansion; §2.2). In the near-wall region, again destruction $-\varepsilon_{zz}^+$ (loss $\forall y^+$) is balanced by viscous diffusion $d_{zz}^{(\mu)+}$ (gain $\forall y^+ \lesssim 6$), but this zone extends further away from the wall ($y^+ \lesssim 3$; Fig. 5) compared to the streamwise

| | | | | | | | | | | | |
|---------------|----------------|-----------------------------|---|--------------|----------------|-------------------|-------------------|--------------|--------------|-------------|----------------|
| Re_{τ_w} | \bar{M}_{CL} | $N_x \times N_y \times N_z$ | $L_x \times L_y \times L_z$ | Δx^+ | Δy_w^+ | $N_{y^+ \leq 10}$ | Δy_{CL}^+ | Δz^+ | Δt^+ | t_{OBS}^+ | Δt_s^+ |
| 182 | 0.35 | $401 \times 201 \times 401$ | $4\pi\delta \times 2\delta \times \frac{4}{3}\pi\delta$ | 5.7 | 0.22 | 26 | 3.1 | 1.9 | 0.0060 | 777 | 0.0060 |

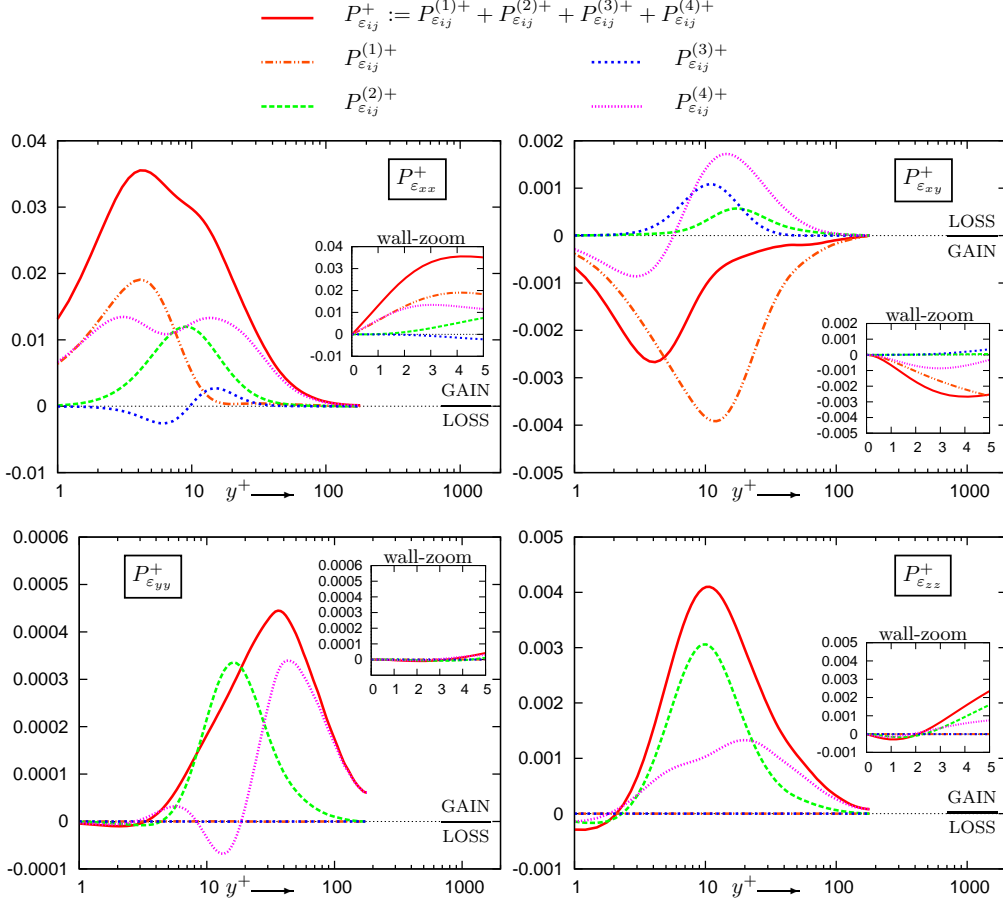


FIGURE 6. Comparison of the various mechanisms of production $P_{\epsilon_{ij}} = P_{\epsilon_{ij}}^{(1)} + P_{\epsilon_{ij}}^{(2)} + P_{\epsilon_{ij}}^{(3)} + P_{\epsilon_{ij}}^{(4)}$ (3.3) of the dissipation tensor ϵ_{ij} (1.2a), in wall-units (A 3f), from the present DNS computations of turbulent plane channel flow ($Re_{\tau_w} \approx 182$, $\bar{M}_{CL} \approx 0.35$), plotted against the inner-scaled (A 3c) wall-distance y^+ (logscale and linear wall-zoom).

component ($y^+ \lesssim 1$; Fig. 5). As for the streamwise component, the other mechanisms, $d_{\epsilon_{zz}}^{(u)+}$ and $\Pi_{\epsilon_{zz}}^+$, have a very small contribution to the ϵ_{zz}^+ -budget. Another difference between the streamwise and the spanwise components is that ϵ_{zz}^+ is maximum at the wall decreasing monotonically with y^+ , contrary to ϵ_{xx}^+ (Fig. 5).

The major difference in the budgets of the wall-normal component ϵ_{yy}^+ , compared to the other two diagonal components, is the importance of the pressure term $\Pi_{\epsilon_{yy}}^+$ which is the dominant gain mechanism throughout the channel (Fig. 5), except very near the wall ($y^+ \lesssim \frac{1}{2}$; Fig. 5) where $\Pi_{\epsilon_{yy}}^+ \rightarrow 0$ (wall-asymptotic expansion; §2.2) and, as for ϵ_{xx}^+ and ϵ_{zz}^+ , viscous diffusion $d_{\epsilon_{yy}}^{(\mu)+}$ (gain) balances destruction $-\epsilon_{\epsilon_{yy}}^+$ ($y^+ \lesssim \frac{1}{2}$; Fig. 5). Production $P_{\epsilon_{yy}}^+$ (gain) is significant in the buffer region ($10 \lesssim y^+ \lesssim 100$; Fig. 5) although it becomes comparable to $\Pi_{\epsilon_{yy}}^+$ only for $y^+ \gtrsim 100$ (Fig. 5). Turbulent diffusion $d_{\epsilon_{yy}}^{(u)+}$ is generally weak throughout the channel (Fig. 5).

| | | | | | | | | | | | |
|---------------|----------------|-----------------------------|---|--------------|----------------|-------------------|-------------------|--------------|--------------|-------------|----------------|
| Re_{τ_w} | \bar{M}_{CL} | $N_x \times N_y \times N_z$ | $L_x \times L_y \times L_z$ | Δx^+ | Δy_w^+ | $N_{y^+ \leq 10}$ | Δy_{CL}^+ | Δz^+ | Δt^+ | t_{OBS}^+ | Δt_s^+ |
| 182 | 0.35 | $401 \times 201 \times 401$ | $4\pi\delta \times 2\delta \times \frac{4}{3}\pi\delta$ | 5.7 | 0.22 | 26 | 3.1 | 1.9 | 0.0060 | 777 | 0.0060 |

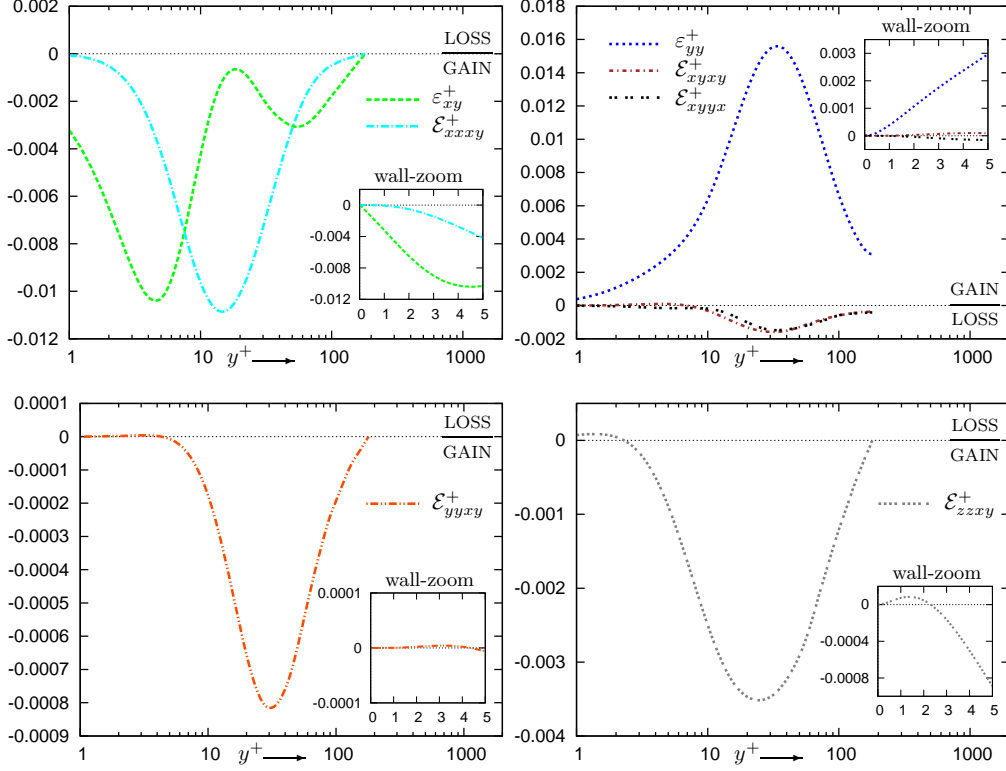


FIGURE 7. Components of ε_{ij} (1.2a) and of $\mathcal{E}_{ijk\ell m}$ (3.1) that appear in the production by mean-velocity-gradient $P_{\varepsilon_{ij}}^{(1)}$ and $P_{\varepsilon_{ij}}^{(2)}$ terms (3.3) of the ε_{ij} -transport budgets expressed for the particular case of fully developed plane channel flow (Tab. 3), in wall-units (A 3e), from the present DNS computations of turbulent plane channel flow ($Re_{\tau_w} \approx 182$, $\bar{M}_{CL} \approx 0.35$), plotted against the inner-scaled (A 3c) wall-distance y^+ (logscale and linear wall-zoom).

| | | |
|--|--|--|
| $P_{\varepsilon_{xx}}^{(1)} = -2\rho\varepsilon_{xy}\frac{d\bar{u}}{dy}$ | $P_{\varepsilon_{xx}}^{(2)} = -2\rho\mathcal{E}_{xxxy}\frac{d\bar{u}}{dy}$ | $P_{\varepsilon_{xx}}^{(3)} = -4\rho\nu v'\overline{\frac{\partial u'}{\partial y}}\frac{d^2\bar{u}}{dy^2}$ |
| $P_{\varepsilon_{xy}}^{(1)} = -\rho\varepsilon_{yy}\frac{d\bar{u}}{dy}$ | $P_{\varepsilon_{xy}}^{(2)} = -\rho(\mathcal{E}_{xyxy} + \mathcal{E}_{xyyx})\frac{d\bar{u}}{dy}$ | $P_{\varepsilon_{xy}}^{(3)} = -\rho 2\nu v'\overline{\frac{\partial v'}{\partial y}}\frac{d^2\bar{u}}{dy^2}$ |
| $P_{\varepsilon_{yy}}^{(1)} = 0$ | $P_{\varepsilon_{yy}}^{(2)} = -2\rho\mathcal{E}_{yyxy}\frac{d\bar{u}}{dy}$ | $P_{\varepsilon_{yy}}^{(3)} = 0$ |
| $P_{\varepsilon_{zz}}^{(1)} = 0$ | $P_{\varepsilon_{zz}}^{(2)} = -2\rho\mathcal{E}_{zzxy}\frac{d\bar{u}}{dy}$ | $P_{\varepsilon_{zz}}^{(3)} = 0$ |

TABLE 3. Components of different mechanisms of production $P_{\varepsilon_{ij}} = P_{\varepsilon_{ij}}^{(1)} + P_{\varepsilon_{ij}}^{(2)} + P_{\varepsilon_{ij}}^{(3)} + P_{\varepsilon_{ij}}^{(4)}$ (3.3) for fully developed turbulent plane channel.

The budgets of the shear component $\varepsilon_{xy}^+ < 0 \forall y^+ > 0$ (Mansour *et al.* 1988, Fig. 4, p. 19) exhibit a fundamentally different behaviour compared to the diagonal components (Fig. 5). All of the terms in the ε_{xy}^+ -budgets ($P_{\varepsilon_{xy}}^+$, $\Pi_{\varepsilon_{xy}}^+$, $d_{\varepsilon_{xy}}^{(u)+}$, $d_{\varepsilon_{xy}}^{(\mu)+}$, $-\varepsilon_{\varepsilon_{xy}}^+$) are significant (Fig. 5). Contrary to the diagonal components, the destruction term $-\varepsilon_{\varepsilon_{xy}}^+$ contributes as gain to the budgets in the major part of the channel ($y^+ \gtrsim 3$; Fig. 5), becoming an actual destruction mechanism (loss) only in the viscous sublayer ($y^+ \lesssim 3$; Fig. 5). Notice that, at the wall, viscous diffusion of the shear component is substantially weaker than the 2 other mechanisms present in (3.3), *viz* $\left| \Pi_{\varepsilon_{xy}}^+ \right|_w \gg \left| d_{\varepsilon_{xy}}^{(\mu)+} \right|_w = \left| \varepsilon_{\varepsilon_{xy}}^+ - \Pi_{\varepsilon_{xy}}^+ \right|_w \ll \left| \varepsilon_{\varepsilon_{xy}}^+ \right|_w$ (wall-asymptotic expansion; §2.2; Fig. 5). In a large part of the channel, $-\varepsilon_{\varepsilon_{xy}}^+ < 0 \forall y^+ \gtrsim 3$ (Fig. 5) is an important gain mechanism, along with production $P_{\varepsilon_{xy}}^+ < 0 \forall y^+ > 0$ (Fig. 5). On the other hand, $\Pi_{\varepsilon_{xy}}^+$ is the main loss mechanism in the major part of the channel (Fig. 5). Notice the complicated y^+ -evolution of $\Pi_{\varepsilon_{xy}}^+$ (Fig. 5), which is < 0 (gain) at the wall, crossing to > 0 (loss) at $y^+ \gtrsim \frac{1}{2}$, and presents a plateau ($3 \lesssim y^+ \lesssim 7$) followed by a global maximum at $y^+ \approx 15$, before decreasing monotonically to 0 at the centerline. In the region $1 \lesssim y^+ \lesssim 20$, both diffusion mechanisms, $d_{\varepsilon_{xy}}^{(\mu)+}$ and $d_{\varepsilon_{xy}}^{(u)+}$, contribute significantly to the ε_{xy} -budgets (Fig. 5).

A major difference between the r_{ij} -budgets (Mansour *et al.* 1988) and the ε_{ij} -budgets (Fig. 5) lies in the production mechanisms P_{ij} (1.1) and $P_{\varepsilon_{ij}}$ (3.3). In the r_{ij} -budgets of plane channel flow, only $P_{xx}^+ \neq 0 \neq P_{xy}^+$ whereas $P_{yy}^+ = P_{zz}^+ = 0 \forall y^+$ (Mansour *et al.* 1988, Figs. 2 and 3, pp. 18–19). On the contrary, all of the components $P_{\varepsilon_{ij}}^+ \neq 0 \forall y^+ > 0$ in general (Fig. 5). In relation to the above observation, the main gain mechanism in the ε_{zz}^+ -budgets is production $P_{\varepsilon_{zz}}^+$ (Fig. 5) in contrast to the r_{zz} -budgets (Mansour *et al.* 1988, Fig. 3, p. 19) where, in the absence of production $P_{zz}^+ = 0 \forall y^+$, the pressure term Π_{zz}^+ is the main gain mechanism. On the contrary, $\Pi_{\varepsilon_{zz}}^+$ has negligible contribution to the ε_{zz} -budgets (Fig. 5). It is noteworthy that the importance of the pressure terms $\Pi_{\varepsilon_{yy}}^+$ and $\Pi_{\varepsilon_{xy}}^+$ in the budgets of the ε_{yy} and ε_{xy} components (Fig. 5) is also quite generally observed in the budgets of wall-normal fluxes, including the Reynolds stresses r_{yy}^+ (Mansour *et al.* 1988, Fig. 2, p. 18) and r_{xy}^+ (Mansour *et al.* 1988, Fig. 4, p. 19), and in the compressible case, the fluxes of thermodynamic quantities such as temperature $\overline{T'v'}$ (Gerolymos & Vallet 2014, Figs. 14 and 15, pp. 737–738), density $\overline{\rho'v'}$ (Gerolymos & Vallet 2014, Fig. 12, p. 731), pressure $\overline{p'v'}$ (Gerolymos & Vallet 2014, Fig. 16, p. 741) and entropy $\overline{s'v'}$ (Gerolymos & Vallet 2014, Fig. 13, p. 734).

Production $P_{\varepsilon_{ij}}^+$ (Fig. 5) of ε_{ij} contains 4 different mechanisms, $P_{\varepsilon_{ij}}^+ = P_{\varepsilon_{ij}}^{(1)+} + P_{\varepsilon_{ij}}^{(2)+} + P_{\varepsilon_{ij}}^{(3)+} + P_{\varepsilon_{ij}}^{(4)+}$ (3.3), which behave differently for each component across the channel (Fig. 6). Globally, in plane channel flow, $P_{\varepsilon_{ij}}^+$ contributes as a gain mechanism in the ε_{ij} -budgets (Figs. 5, 6), except very near the wall for the wall-normal ($P_{\varepsilon_{yy}}^+ \leq 0 \forall y^+ \lesssim 3$ is a loss mechanism; Fig. 5) and spanwise ($P_{\varepsilon_{zz}}^+ \leq 0 \forall y^+ \lesssim 2$ is a loss mechanism; Fig. 5) diagonal components. For both the spanwise and wall-normal components, $P_{\varepsilon_{yy}}^{(1)+} = P_{\varepsilon_{zz}}^{(1)+} = P_{\varepsilon_{yy}}^{(3)+} = P_{\varepsilon_{zz}}^{(3)+} = 0 \forall y^+$ (Tab. 3), whereas production by the action of \mathcal{E}_{ijk}^+ -components on the mean velocity-gradient, $P_{\varepsilon_{yy}}^{(2)+}$ and $P_{\varepsilon_{zz}}^{(2)+}$ (Tab. 3), is the main gain mechanism in the initial part of the buffer layer ($y^+ \in [5, 30]$; Fig. 6) and is replaced further away from the wall ($y^+ \gtrsim 30$; Fig. 6) by production by triple correlations of fluctuating velocity-gradients, $P_{\varepsilon_{yy}}^{(4)+}$ and $P_{\varepsilon_{zz}}^{(4)+}$ (3.3), as expected from the quasi-homogeneous analysis of Tennekes & Lumley (1972, pp. 88–92). All of the 4 production mechanisms (3.3) are active for the streamwise ε_{xx}^+ and shear ε_{xy}^+ components (Fig. 6). Regarding the streamwise component ε_{xx}^+ , the 3 mechanisms, $P_{\varepsilon_{xx}}^{(1)+} > 0$,

$P_{\varepsilon_{xx}}^{(2)+} > 0$ and $P_{\varepsilon_{xx}}^{(4)+} > 0 \forall y^+ > 0$ (Fig. 6) always contribute as gain to the budgets. On the other hand, production by the mean velocity-Hessian, $P_{\varepsilon_{xx}}^{(3)+} < 0 \forall y^+ \lesssim 10$ (loss) near the wall (Fig. 6), switching to $P_{\varepsilon_{xx}}^{(3)+} > 0 \forall y^+ \gtrsim 10$ (gain) further away from the wall, is generally weaker than the other 3 mechanisms. Notice that the production by the triple correlations of the fluctuating velocity-gradients $P_{\varepsilon_{xx}}^{(4)+}$ (3.3) is important throughout the channel, even as $y^+ \rightarrow 0$ (Fig. 6), becoming the dominant mechanism in the outer part of the flow ($y^+ \gtrsim 15$; Fig. 6). Regarding the shear component ε_{xy}^+ , $P_{\varepsilon_{xy}}^{(1)+} = -\varepsilon_{yy}^+[d_y \bar{u}]^+ < 0 \forall y^+ > 0$ (Fig. 6) is the main gain mechanism throughout the channel, whereas $P_{\varepsilon_{xy}}^{(2)+} > 0$ and $P_{\varepsilon_{xy}}^{(3)+} > 0 \forall y^+ > 0$ contribute as loss to the budgets (Fig. 6). Finally, $P_{\varepsilon_{xy}}^{(4)+} < 0 \forall y^+ \lesssim 6$ (gain) near the wall (Fig. 6) switches to $P_{\varepsilon_{xy}}^{(4)+} > 0 \forall y^+ \gtrsim 6$ (loss) further away from the wall. Interestingly, $P_{\varepsilon_{xy}}^{(4)+}$, although comparable to the other 3 mechanisms $\forall y^+$ (Fig. 6), never becomes the dominant mechanism, even as $y^+ \rightarrow \delta^+$, raising the question of applicability of the quasi-homogeneous order-of-magnitude analysis (Tennekes & Lumley 1972, pp. 88–92) to the shear component (although higher- Re data are required to fully resolve this issue).

In plane channel flow, production by interaction with the mean velocity-gradient $P_{\varepsilon_{ij}}^{(1)+} + P_{\varepsilon_{ij}}^{(2)+}$ (3.3) involves ε_{xy}^+ in $P_{\varepsilon_{xx}}^{(1)+}$ (Tab. 3), ε_{yy}^+ in $P_{\varepsilon_{yy}}^{(1)+}$ (Tab. 3), and 5 different components of $\mathcal{E}_{ijk m}$ (3.1) in $P_{\varepsilon_{ij}}^{(2)+}$ (Tab. 3), which are not involved in the generating relation (3.1a). Since the mean velocity-gradient $d_y \bar{u}^+ > 0 \forall y^+ \in]0, \delta^+[$ (Coles 1956), the sign of these components directly determines (Tab. 3) whether the corresponding contribution to $P_{\varepsilon_{ij}}^+$ is gain or loss (Figs. 6, 7).

Concerning $P_{\varepsilon_{xx}}^{(1)+}$ and $P_{\varepsilon_{xx}}^{(2)+}$ (Tab. 3), the corresponding producing components, ε_{xy}^+ and \mathcal{E}_{xxxy}^+ are of comparable magnitude (Fig. 7), but ε_{xy}^+ is active nearer to the wall (peak at $y^+ \in [4, 5]$; Fig. 7) compared to \mathcal{E}_{xxxy}^+ (peak at $y^+ \approx 15$; Fig. 7). Therefore, $P_{\varepsilon_{xx}}^{(1)+}$ peaks at $y^+ \in [4, 5]$ whereas $P_{\varepsilon_{xx}}^{(2)+}$ peaks at $y^+ \approx 9$ (Fig. 6). Near the wall (wall-asymptotic expansion; §2.2), $P_{\varepsilon_{xx}}^{(2)+} \underset{y^+ \rightarrow 0}{\sim} O(y^{+2})$ whereas $P_{\varepsilon_{xx}}^{(1)+} \underset{y^+ \rightarrow 0}{\sim} O(y^+)$ (Fig. 6). For the wall-normal and spanwise diagonal components $P_{\varepsilon_{yy}}^{(1)+} = P_{\varepsilon_{zz}}^{(1)+} = 0$ (Tab. 3), so that only $P_{\varepsilon_{yy}}^{(2)+}$ and $P_{\varepsilon_{zz}}^{(2)+}$ appear in the budgets of ε_{yy}^+ and ε_{zz}^+ respectively (Fig. 6), with corresponding producing components \mathcal{E}_{yyxy}^+ and \mathcal{E}_{zzxy}^+ respectively (Tab. 3). These components peak at $y^+ \approx 30$ (\mathcal{E}_{yyxy}^+ ; Fig. 7) and $y^+ \approx 25$ (\mathcal{E}_{zzxy}^+ ; Fig. 7), the \mathcal{E}_{zzxy}^+ -peak being larger than the \mathcal{E}_{yyxy}^+ -peak (Fig. 7). The producing component $\mathcal{E}_{yyxy}^+ \gtrsim 0 \forall y^+ > 0$ (Fig. 7), so that (Tab. 3) $P_{\varepsilon_{yy}}^{(2)+} \gtrsim 0 \forall y^+ > 0$ (gain; Fig. 6) with a peak at $y^+ \approx 18$. On the other hand, $\mathcal{E}_{zzxy}^+ < 0 \forall y^+ \gtrsim 2$ (gain; Fig. 7) changes sign near the wall ($\mathcal{E}_{zzxy}^+ > 0 \forall y^+ \lesssim 2$; loss; Fig. 7). Regarding the shear component ε_{xy}^+ , the producing terms $\varepsilon_{yy}^+ > 0 \forall y^+ > 0$ (Fig. 7) in $P_{\varepsilon_{xy}}^{(1)+}$ (Tab. 3) and $(\mathcal{E}_{xyxy}^+ + \mathcal{E}_{xyyx}^+) \lesssim 0 \forall y^+ > 0$ (Fig. 7) in $P_{\varepsilon_{xy}}^{(2)+}$ (Tab. 3), so that $P_{\varepsilon_{xy}}^{(2)+} \gtrsim 0 \forall y^+ > 0$ (loss; Fig. 6) opposes, but is weaker than, $P_{\varepsilon_{xy}}^{(1)+} \lesssim 0 \forall y^+ > 0$ (gain; Fig. 6).

4. Re_{τ_w} influence on ε_{ij} -budgets

The previous analysis of ε_{ij} (§3) concerned the low $Re_{\tau_w} \approx 180$ case. It turns out that the data of Vreman & Kuerten (2014a,b, 2016) for the budgets of the transport equations for the 9 components of the velocity-gradient variance $(\partial_{x_j} u_i')^2$ (Vreman & Kuerten 2014b, (9–18), p. 4) can be combined to yield the budgets of the transport equations of the diagonal components $\{\varepsilon_{xx}^+, \varepsilon_{yy}^+, \varepsilon_{zz}^+\}$ for $Re_{\tau_w} \in \{180, 590\}$ (Figs. 8, 9).

| Re_{τ_w} | \bar{M}_{CL} | $N_x \times N_y \times N_z$ | $L_x \times L_y \times L_z$ | Δx^+ | Δy_w^+ | $N_{y^+ \leq 10}$ | Δy_{CL}^+ | Δz^+ | Δt^+ | t_{OBS}^+ | Δt_s^+ | |
|---------------|----------------|-----------------------------|---|--------------|----------------|-------------------|-------------------|--------------|--------------|-------------|----------------|-------------------------|
| 182 | 0.35 | $401 \times 201 \times 401$ | $4\pi\delta \times 2\delta \times \frac{4}{3}\pi\delta$ | 5.7 | 0.224 | 26 | 3.1 | 1.9 | 0.0066 | 777 | 0.0066 | present |
| 180 | 0 | $384 \times 385 \times 192$ | $4\pi\delta \times 2\delta \times \frac{4}{3}\pi\delta$ | 5.9 | 0.006 | 42 | 1.5 | 3.9 | 0.0150 | 36000 | 11.2500 | Vreman & Kuerten (2016) |
| 590 | 0 | $768 \times 385 \times 768$ | $2\pi\delta \times 2\delta \times \pi\delta$ | 4.8 | 0.020 | 24 | 4.8 | 2.4 | 0.0738 | 59000 | 18.4325 | Vreman & Kuerten (2014) |

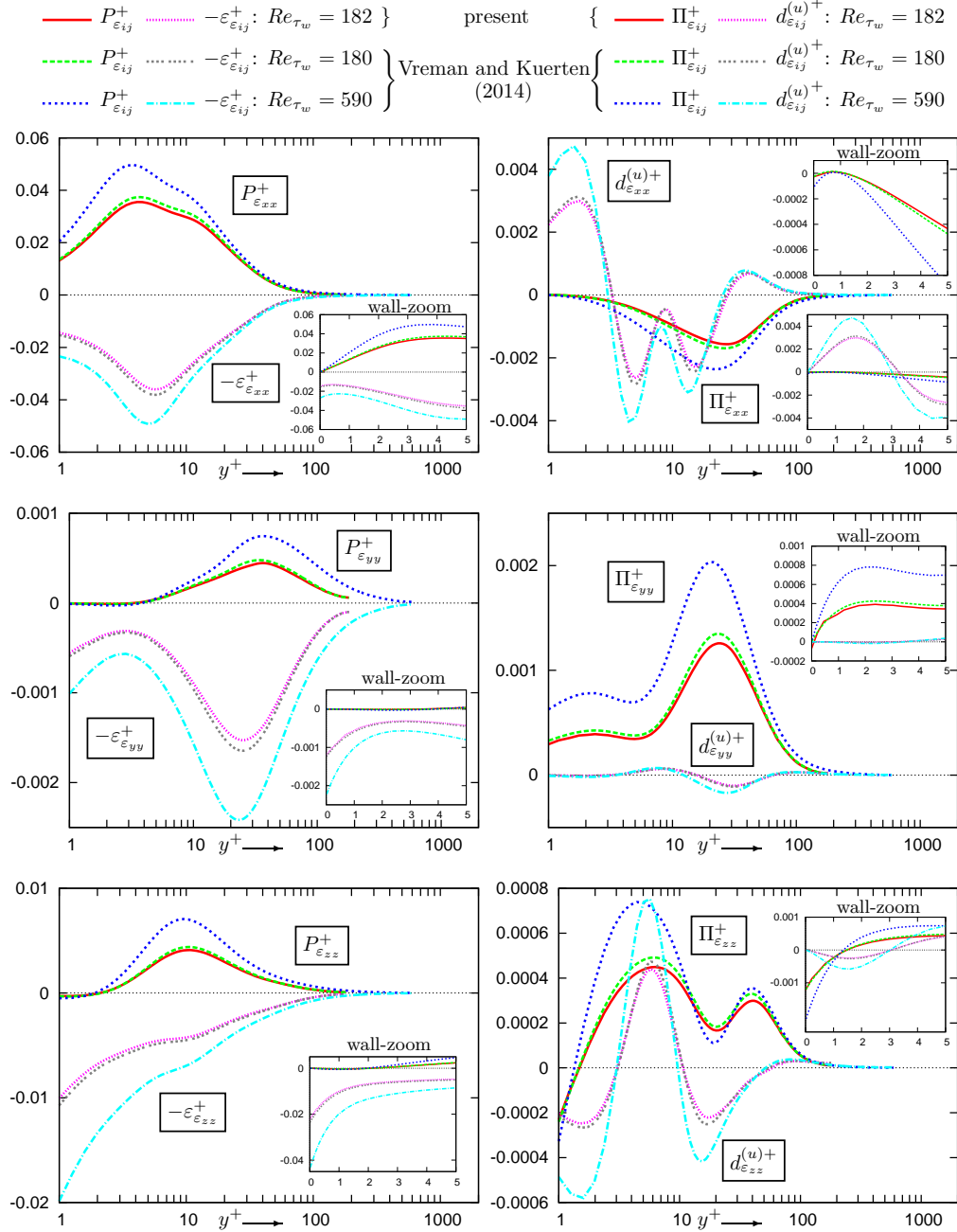


FIGURE 8. Examination of the influence of the Reynolds number Re_{τ_w} (A 3g) on various terms ($P_{\varepsilon_{ij}}$, $\varepsilon_{\varepsilon_{ij}}$, $\Pi_{\varepsilon_{ij}}$, and $d_{\varepsilon_{ij}}^{(u)}$) in the budgets of the transport equations (3.3) for the diagonal components of the dissipation tensor ε_{ij} (1.2a), in wall-units (A 3f), by comparison of the present DNS computations of turbulent plane channel flow ($Re_{\tau_w} \approx 182$, $\bar{M}_{CL} \approx 0.35$) with the incompressible DNS data of Vreman & Kuerten (2014a,b, 2016, $Re_{\tau_w} \in \{180, 590\}$, $\bar{M}_{CL} = 0$) plotted against the inner-scaled (A 3c) wall-distance y^+ (logscale and linear wall-zoom).

| Re_{τ_w} | \bar{M}_{CL} | $N_x \times N_y \times N_z$ | $L_x \times L_y \times L_z$ | Δx^+ | Δy_w^+ | $N_{y^+ \leq 10}$ | Δy_{CL}^+ | Δz^+ | Δt^+ | t_{OBS}^+ | Δt_s^+ | |
|---------------|----------------|-----------------------------|---|--------------|----------------|-------------------|-------------------|--------------|--------------|-------------|----------------|-------------------------|
| 182 | 0.35 | $401 \times 201 \times 401$ | $4\pi\delta \times 2\delta \times \frac{4}{3}\pi\delta$ | 5.7 | 0.224 | 26 | 3.1 | 1.9 | 0.0066 | 777 | 0.0066 | present |
| 180 | 0 | $384 \times 385 \times 192$ | $4\pi\delta \times 2\delta \times \frac{4}{3}\pi\delta$ | 5.9 | 0.006 | 42 | 1.5 | 3.9 | 0.0150 | 36000 | 11.2500 | Vreman & Kuerten (2016) |
| 590 | 0 | $768 \times 385 \times 768$ | $2\pi\delta \times 2\delta \times \pi\delta$ | 4.8 | 0.020 | 24 | 4.8 | 2.4 | 0.0738 | 59000 | 18.4325 | Vreman & Kuerten (2014) |

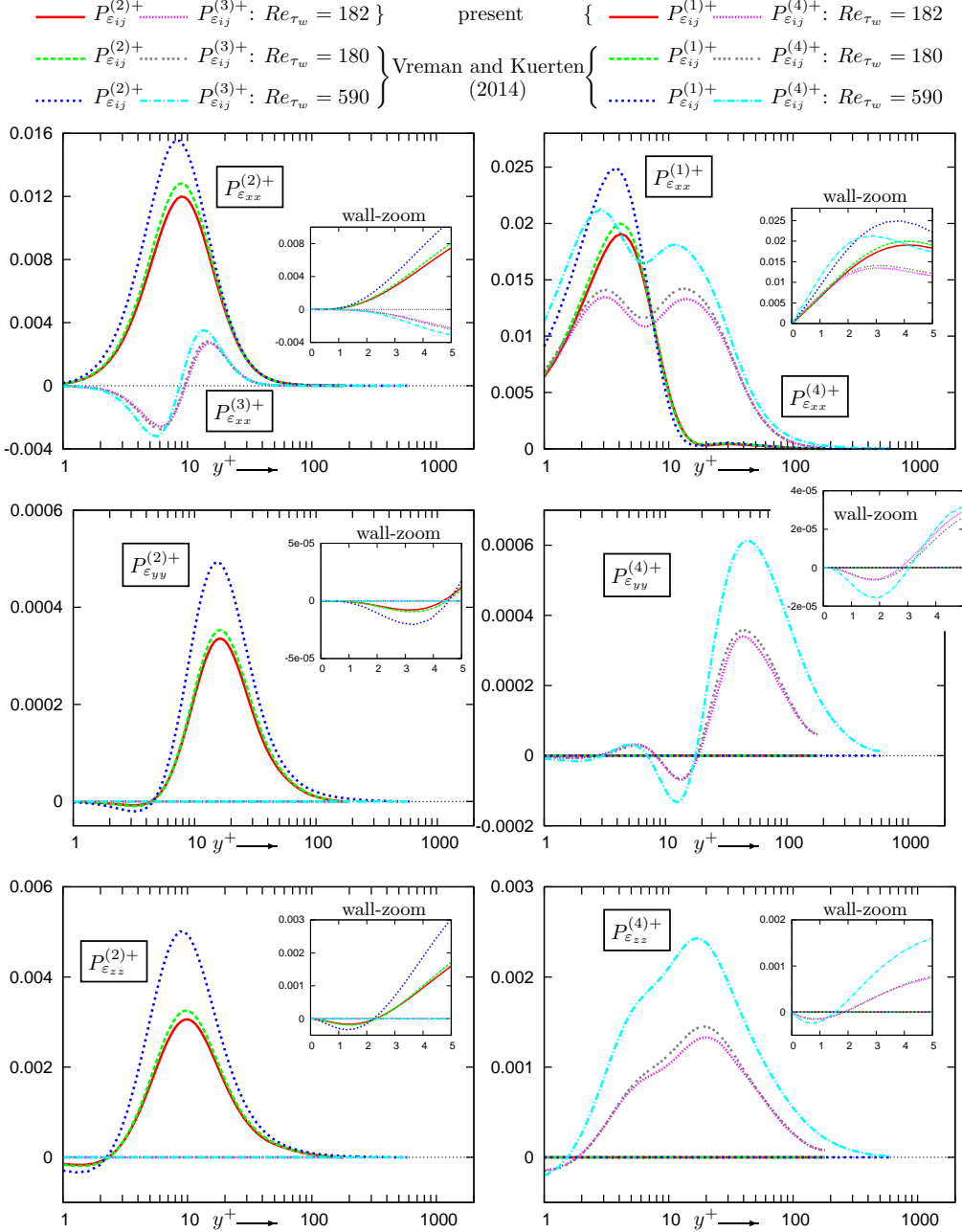


FIGURE 9. Examination of the influence of the Reynolds number Re_{τ_w} (A 3g) on the of production $P_{\varepsilon_{ij}} = P_{\varepsilon_{ij}}^{(1)} + P_{\varepsilon_{ij}}^{(2)} + P_{\varepsilon_{ij}}^{(3)} + P_{\varepsilon_{ij}}^{(4)}$ (3.3) of the diagonal components of the dissipation tensor ε_{ij} (1.2a), in wall-units (A 3f), by comparison of the present DNS computations of turbulent plane channel flow ($Re_{\tau_w} \approx 182$, $\bar{M}_{CL} \approx 0.35$) with the incompressible DNS data of Vreman & Kuerten (2014a,b, 2016, $Re_{\tau_w} \in \{180, 590\}$, $\bar{M}_{CL} = 0$) plotted against the inner-scaled (A 3c) wall-distance y^+ (logscale and linear wall-zoom).

Unfortunately, data for the budgets of the transport equation for the shear component ε_{xy}^+ could not be obtained from this database. The data of Vreman & Kuerten (2014a,b, 2016) were sampled at much lower frequencies ($\Delta t_s^+ \in \{11.25, 18.43\}$) but for much longer observation times ($t_{\text{OBS}}^+ \in \{36000, 59000\}$).

With regard to the lower Reynolds number $Re_{\tau_w} \cong 180$, the agreement between the present $\bar{M}_{\text{CL}} \cong 0.35$ aerodynamic DNS data and the incompressible DNS data of Vreman & Kuerten (2016) is excellent, the 2 sets of data practically collapsing on the same curves (Figs. 8, 9). This agreement between completely different computational approaches and flow models (Gerolymos *et al.* 2010; Vreman & Kuerten 2016), spatial (in particular y -wise) and temporal resolutions, and averaging times (Figs. 8, 9), both strengthens considerably the confidence in the data and corroborates the analysis of weak-density-fluctuation effects (Gerolymos *et al.* 2013, Appendix A, pp. 45–51), showing that compressibility effects on turbulence structure are indeed negligible for $\bar{M}_{\text{CL}} \lesssim 0.35$, in line with the finding that $\rho'_{\text{rms}} \propto \bar{\rho} \bar{M}_{\text{CL}}^2$ (Gerolymos & Vallet 2014, Fig. 5, p. 720).

Regarding the influence of Re_{τ_w} on the diagonal components of various terms ($P_{\varepsilon_{ij}}$, $\varepsilon_{\varepsilon_{ij}}$, $\Pi_{\varepsilon_{ij}}$, and $d_{\varepsilon_{ij}}^{(u)}$) in the ε_{ij} -budgets (3.3), although the level of wall-values and of different peaks present in the wall-normal (y -wise) distributions are higher with increasing Reynolds number (Figs. 8, 9), there are no significant qualitative differences. However, the locations and/or values of some near-wall extrema exhibit substantial variation as Re_{τ_w} increases from 180 to 590. These variations are analogous to the observed behaviour of near-wall anisotropy (Figs. 1–3), but this analogy also suggests that lesser influence should be expected as Re_{τ_w} further increases above 590. Regarding the location of near-wall extrema of different terms there is a general trend (Figs. 8, 9) that they occur at lower y^+ (closer to the wall) as Re_{τ_w} increases from 180 to 590. Notice, however, that the very-near-wall location where the streamwise and spanwise components of the destruction-of-dissipation tensor $\varepsilon_{\varepsilon_{xx}} = \varepsilon_{\varepsilon_{zz}}$, exhibits the opposite behaviour, very slightly increasing from $y^+ \cong 0.6$ at $Re_{\tau_w} = 180$ to $y^+ \cong 0.8$ at $Re_{\tau_w} = 590$. Another noticeable Re_{τ_w} -effect is the difference of the near-wall levels of the wall-normal and spanwise components of the destruction-of-dissipation tensor, $\varepsilon_{\varepsilon_{yy}}$ and $\varepsilon_{\varepsilon_{zz}}$, which are at $Re_{\tau_w} = 590$ nearly twice those observed at $Re_{\tau_w} = 180$ (Fig. 8).

5. Conclusions

Available and novel DNS data were used to study the positive-definite dissipation tensor ε_{ij} (1.2a), representing the destruction of the Reynolds-stresses r_{ij} (2.1a) by the action of molecular viscosity, in wall turbulence, and in particular its anisotropy and transport-equations budgets.

Taylor-expansions of the fluctuating velocities in the neighbourhood of a plane no-slip xz -wall show that, for incompressible turbulent flow, the wall-normal gradients of the ε_{ij} -anisotropy tensor $b_{\varepsilon_{ij}}$ and of its invariants, at the wall, are exactly twice the wall-normal gradients of the corresponding components and invariants of the Reynolds-stress anisotropy tensor b_{ij} . Furthermore, both the dissipation tensor ε_{ij} and the Reynolds-stress tensor r_{ij} , depart from the 2-C state at the wall (flatness parameter $A_w = A_{\varepsilon_w} = 0$) quadratically with wall-distance y^+ ($A_{\varepsilon} \sim_{y^+ \rightarrow 0} 4A \sim_{y^+ \rightarrow 0} O(y^{+2})$).

Available DNS data suggest several general trends in the anisotropy of r_{ij} and ε_{ij} , with varying Reynolds number Re_{τ_w} . The y^+ -wise distributions of the components and invariants of the Reynolds-stress anisotropy tensor b_{ij} develop, as Re_{τ_w} increases, a plateau, roughly corresponding to the log-layer of the mean velocity profile, followed by a wake-like region in the outer part near the centerline. At the centerline, DNS data show quite consis-

tently that b_{ij} reaches a rod-like axisymmetric componentality, at least for $Re_{\tau_w} \gtrsim 180$. On the contrary, the components and invariants of $b_{\varepsilon_{ij}}$ seem, as Re_{τ_w} increases, to vary smoothly from $y^+ \approx 100$ to the centerline, where ε_{ij} is not axisymmetric. Interestingly, at the low Re_{τ_w} limit, the anisotropy invariants ($-\Pi_{\mathbf{b}}$, $\text{III}_{\mathbf{b}}$, $-\Pi_{\mathbf{b}_e}$, $\text{III}_{\mathbf{b}_e}$) seem to increase continuously, with decreasing Re_{τ_w} , both at the wall and at the centerline.

The dissipation tensor ε_{ij} (1.2a), is governed by transport equations (3.3) where convection by the mean-flow $C_{\varepsilon_{ij}}$ is balanced by the usual mechanisms: molecular diffusion $d_{\varepsilon_{ij}}^{(\mu)}$, turbulent diffusion $d_{\varepsilon_{ij}}^{(u)}$, production $P_{\varepsilon_{ij}}$ the effect of the fluctuating pressure-Hessian $\Pi_{\varepsilon_{ij}}$, and destruction by molecular viscosity $\varepsilon_{\varepsilon_{ij}}$.

Budgets for these equations were studied using DNS results for low $Re_{\tau_w} \approx 180$ turbulent plane channel flow (for this particular flow convection $C_{\varepsilon_{ij}} = 0$). As expected, since ε_{ij} is the footprint of the behaviour of the small turbulent scales, the various mechanisms in the ε_{ij} -budgets behave unlike the corresponding mechanisms in the r_{ij} -budgets (Mansour *et al.* 1988). Production $P_{\varepsilon_{ij}}$ is significant (gain) for all of the ε_{ij} -components, contrary to the r_{ij} -budgets, where for plane channel flow $P_{yy} = P_{zz} = 0 \forall y^+$. On the other hand, the pressure term $\Pi_{\varepsilon_{ij}}$ is significant in the budgets of the wall-normal ($\Pi_{\varepsilon_{yy}}$) and shear ($\Pi_{\varepsilon_{xy}}$) components and negligibly small in the budgets of the streamwise ($\Pi_{\varepsilon_{xx}}$) and spanwise ($\Pi_{\varepsilon_{zz}}$) components. This contrasts with the r_{ij} -budgets, where Π_{zz} is the main gain mechanism in the ($r_{zz} := \overline{w'^2}$)-budgets and Π_{xx} , although relatively weak near the wall, is an important loss mechanism for $y^+ \gtrsim 20$ in the ($r_{xx} := \overline{u'^2}$)-budgets (Mansour *et al.* 1988). Production of the diagonal components (ε_{xx} , ε_{yy} and ε_{zz}) by the triple correlations of the fluctuating velocity-gradients $P_{\varepsilon_{ij}}^{(4)}$ is the main gain mechanism, in line with quasi-homogeneous theory (Tennekes & Lumley 1972, pp. 88–92), only away from the wall ($y^+ \gtrsim 20$), but this does not apply for the shear component ε_{xy} , for which $P_{\varepsilon_{xy}}^{(4)}$ is a loss mechanism in the major part of the channel ($y^+ \gtrsim 6$). The budgets of the diagonal components (ε_{xx} , ε_{yy} and ε_{zz}) were also evaluated at higher $Re_{\tau_w} \approx 590$, by combining available DNS data of Vreman & Kuerten (2014b) for the variances of the fluctuating velocity-gradient components, showing both the same qualitative behaviour as for the lower $Re_{\tau_w} \approx 180$ case and higher values of the different peaks.

In addition to the ubiquitous effort to extend the DNS results to higher Reynolds numbers, there are several new research directions suggested by the present results, which are the subject of ongoing work: (a) investigate the dynamics and transport-equation budgets of the destruction-of-dissipation tensor $\varepsilon_{\varepsilon_{ij}}$ in an effort to understand the very-small-scale inhomogeneity information it represents, (b) complete the very-low $Re_{\tau_w} \lesssim 100$ range of DNS data to further substantiate and investigate the specific anisotropy behaviour observed in the Hu *et al.* (2002, 2003, 2006) channel data, and (c) to exploit the DNS database for the development and assessment of complete r_{ij} - ε_{ij} second-moment closures, which by including transport equations for all the components of the lengthscale tensor are better adapted to the strong inhomogeneity-induced anisotropy of practical turbulent wall-bounded flows.

The authors are listed alphabetically. The present work was partly funded by the ANR project N_{um}ERICCS(ANR-15-CE06-0009). Computations were performed using HPC ressources allocated at GENCI-IDRIS (Grant 2015-022139) and at ICS-UPMC (ANR-10-EQPX-29-01). Tabulated data are available at http://www.aerodynamics.fr/DNS_database/CT.chnnl.

Appendix. Asymptotic behaviour in the viscous sublayer ($y^+ \rightarrow 0$)

Assume turbulent flow near a plane wall, coincident with the xz -plane and located at $y^+ = 0$. Near the wall, all fluctuating quantities are expanded y -wise in Taylor-series around $y^+ = 0$

$$\begin{aligned} (\cdot)'_{y^+ \rightarrow 0} \sim & (\cdot)'_w(x^+, z^+, t^+) + A'_{(\cdot)}(x^+, z^+, t^+) y^+ + B'_{(\cdot)}(x^+, z^+, t^+) y^{+2} \\ & + C'_{(\cdot)}(x^+, z^+, t^+) y^{+3} + D'_{(\cdot)}(x^+, z^+, t^+) y^{+4} + \dots \end{aligned} \quad (\text{A } 1)$$

with coefficients proportional to the wall-normal (y) derivatives of the appropriate order, which are stationary random functions of $\{x^+, z^+, t^+\}$. The limiting behaviour in the viscous sublayer is determined by the no-slip condition at the wall Mansour *et al.* (1988).

$$y^+ \in \{0, 2\delta^+\} \implies \bar{u}^+ = \bar{v}^+ = \bar{w}^+ = u'^+ = v'^+ = w'^+ = 0 \quad ; \quad \forall x^+, z^+, t^+ \quad (\text{A } 2)$$

A.1. Wall units

All variables are made nondimensional using the mean wall shear stress, the constant fluid density ρ and the constant dynamic viscosity ν

$$\bar{\tau}_w := [\bar{\tau}_{xy}]_w \quad ; \quad \rho \cong \text{const} \quad ; \quad \nu \cong \text{const} \quad (\text{A } 3a)$$

which define the friction-velocity

$$u_\tau := \sqrt{\frac{\bar{\tau}_w}{\rho}} \quad (\text{A } 3b)$$

where τ_{ij} is the viscous stress tensor (Davidson 2004, (2.4), p. 31). Using wall-units (A 3a, A 3b), the nondimensional variables $(\cdot)^+$ are defined as

$$y^+ := \frac{u_\tau (y - y_w)}{\nu} \quad ; \quad t^+ := \frac{t u_\tau^2}{\nu} \quad ; \quad u_i^+ := \frac{u_i}{u_\tau} \quad (\text{A } 3c)$$

$$[r_{ij}^+, \tau_{ij}^+, p^+]^T := \frac{1}{\rho u_\tau^2} [\rho \overline{u'_i u'_j}, \tau_{ij}, p]^T \quad (\text{A } 3d)$$

$$[\varepsilon_{ij}^+, P_{ij}^+, \Pi_{ij}^+, d_{ij}^+]^T := \frac{\nu}{\rho u_\tau^4} [\rho \varepsilon_{ij}, P_{ij}, \Pi_{ij}, d_{ij}]^T \quad (\text{A } 3e)$$

$$[\varepsilon_{\varepsilon_{ij}}^+, P_{\varepsilon_{ij}}^+, \Pi_{\varepsilon_{ij}}^+, d_{\varepsilon_{ij}}^+]^T := \frac{\nu^2}{\rho u_\tau^6} [\rho \varepsilon_{\varepsilon_{ij}}, P_{\varepsilon_{ij}}, \Pi_{\varepsilon_{ij}}, d_{\varepsilon_{ij}}]^T \quad (\text{A } 3f)$$

ie terms in r_{ij} -transport (1.1) scale as $\rho \nu^{-1} u_\tau^4$ whereas terms in ε_{ij} -transport (3.3) scale as $\rho \nu^{-2} u_\tau^6$ (Jovanović 2004, p. 42). In fully developed turbulent channel flow, the friction Reynolds number is defined as

$$Re_{\tau_w} := \frac{u_\tau \delta}{\nu} \stackrel{(\text{A } 3c)}{=} \delta^+ \quad (\text{A } 3g)$$

where 2δ is the channel's height.

A.2. Anisotropy tensors and invariants

The expansions (2.3) can be used to obtain the expansions for the anisotropy tensors b_{ij} (2.1a) and $b_{\varepsilon_{ij}}$ (2.2a), and their invariants (2.1b, 2.2b). Recall that if

$$P(x) \sim \sum_{m=0}^{\infty} \alpha_m x^m \quad ; \quad Q(x) \sim \sum_{m=0}^{\infty} \beta_m x^m \quad (\text{A } 4a)$$

then the asymptotic expansion of their ratio is given by

$$\begin{aligned} \frac{P(x)}{Q(x)} \sim \sum_{\ell=0}^{\infty} \gamma_{\ell} x^{\ell} &\iff \left(\sum_{\ell=0}^{\infty} \gamma_{\ell} x^{\ell} \right) \left(\sum_{m=0}^{\infty} \beta_m x^m \right) \sim \sum_{n=0}^{\infty} \alpha_n x^n \\ &\iff \sum_{n=0}^{\infty} \left(\left(\sum_{\ell=0}^n \beta_{n-\ell} \gamma_{\ell} \right) - \alpha_n \right) x^n \sim 0 \end{aligned} \quad (\text{A } 4b)$$

resulting in a series of linear relations that can be solved sequentially to obtain the coefficients γ_n . Straightforward calculations yield the wall-asymptotic expansions of the anisotropy tensors \mathbf{b} (Tab. 1) and \mathbf{b}_{ε} (Tab. 2). Substitution of these expansions in (2.1b, 2.2b) yields after straightforward but lengthy calculations the asymptotic expansions for the invariants as $y^+ \rightarrow 0$ (Tabs. 1, 2).

REFERENCES

- DEL ÁLAMO, J. C. & JIMÉNEZ, J. 2003 Spectra of the very large anisotropic scales in turbulent channels. *Phys. Fluids* **15** (6), L41–L44.
- ARIS, R. 1962 *Vectors, Tensors, and the Basic Equations of Fluid Mechanics*. New York [NY, USA]: Dover, (1989 ed.).
- BEN NASR, N., GEROLYMOS, G. A. & VALLET, I. 2014 Low-diffusion approximate Riemann solvers for Reynolds-stress transport. *J. Comp. Phys.* **268**, 186–235.
- BERNARDINI, M., PIROZZOLI, S. & ORLANDI, P. 2014 Velocity statistics in turbulent channel flow up to $Re_{\tau} = 4000$. *J. Fluid Mech.* **742**, 171–191.
- BHATTACHARYA, A., KASSINOS, S. C. & MOSER, R. D. 2008 Representing anisotropy of two-point second-order turbulence velocity correlations using structure tensors. *Phys. Fluids* **20**, 101502(1–13).
- BRADSHAW, P. 1967 The turbulence structure in equilibrium boundary-layers. *J. Fluid Mech.* **29**, 625–645.
- BUSCHMANN, M. H. & GAD-EL-HAK, M. 2007 Recent developments in scaling of wall-bounded flows. *Prog. Aerosp. Sci.* **42**, 419–467.
- CHANG, III, P. A., PIOMELLI, U. & BLAKE, W. K. 1999 Relations between wall-pressure and velocity-field sources. *Phys. Fluids* **11** (11), 3434–3448.
- CHAPMAN, D. R. & KUHN, G. D. 1986 The limiting behaviour of turbulence near a wall. *J. Fluid Mech.* **170**, 265–292.
- CHOU, P. Y. 1945 On velocity correlations and the solutions of the equations of turbulent fluctuations. *Quart. Appl. Math.* **3**, 38–54.
- COLES, D. 1956 The law of the wake in a turbulent boundary layer. *J. Fluid Mech.* **1**, 191–226.
- CRAFT, T. J. & LAUNDER, B. 2001 Principles and performance of TCL-based second-moment closures. *Flow Turb. Comb.* **66**, 355–372.
- DAVIDSON, P. A. 2004 *Turbulence*. Oxford [GBR]: Oxford University Press.
- DURBIN, P. A. & SPEZIALE, C. G. 1991 Local anisotropy in strained turbulence at high reynolds numbers. *ASME J. Fluids Eng.* **113**, 707–709.
- GEROLYMOS, G. A., LO, C. & VALLET, I. 2012a Tensorial representations of Reynolds-stress pressure-strain redistribution. *ASME J. Appl. Mech.* **79** (4), 044506(1–10).
- GEROLYMOS, G. A., LO, C., VALLET, I. & YOUNIS, B. A. 2012b Term-by-term analysis of near-wall second moment closures. *AIAA J.* **50** (12), 2848–2864.
- GEROLYMOS, G. A., SÉNÉCHAL, D. & VALLET, I. 2009 Very-high-order WENO schemes. *J. Comp. Phys.* **228**, 8481–8524.
- GEROLYMOS, G. A., SÉNÉCHAL, D. & VALLET, I. 2010 Performance of very-high-order upwind schemes for DNS of compressible wall-turbulence. *Int. J. Num. Meth. Fluids* **63**, 769–810.
- GEROLYMOS, G. A., SÉNÉCHAL, D. & VALLET, I. 2013 Wall effects on pressure fluctuations in turbulent channel flow. *J. Fluid Mech.* **720**, 15–65.
- GEROLYMOS, G. A. & VALLET, I. 2014 Pressure, density, temperature and entropy fluctuations in compressible turbulent plane channel flow. *J. Fluid Mech.* **757**, 701–746.

- HANJALIĆ, K. 1994 Advanced turbulence closure models: A view of current status and future prospects. *Int. J. Heat Fluid Flow* **15**, 178–203.
- HANJALIĆ, K. & JAKIRLIĆ, S. 1993 A model of stress dissipation in second-moment closures. *Appl. Sci. Res.* **51**, 513–518.
- HINZE, J. O. 1975 *Turbulence*, 2nd edn. New York [NY, USA]: McGraw-Hill.
- HOYAS, S. & JIMÉNEZ, J. 2006 Scaling of the velocity fluctuations in turbulent channels up to $Re_\tau = 2003$. *Phys. Fluids* **18**, 011702(1–4).
- HOYAS, S. & JIMÉNEZ, J. 2008 Reynolds number effects on the Reynolds-stress budgets in turbulent channels. *Phys. Fluids* **20**, 101511(1–8).
- HU, Z. W., MORFEY, C. L. & SANDHAM, N. D. 2002 Aeroacoustics of wall-bounded turbulent flow. *AIAA J.* **40** (3), 465–473.
- HU, Z. W., MORFEY, C. L. & SANDHAM, N. D. 2003 Sound radiation in turbulent channel flows. *J. Fluid Mech.* **475**, 269–302.
- HU, Z. W., MORFEY, C. L. & SANDHAM, N. D. 2006 Wall pressure and shear stress spectra from direct simulations of channel flow. *AIAA J.* **44** (7), 1541–1549.
- JAKIRLIĆ, S., EISFELD, B., JESTER-ZÜRKER, R. & KROLL, N. 2007 Near-wall Reynolds-stress model calculations of transonic flow configurations relevant to aircraft aerodynamics. *Int. J. Heat Fluid Flow* **28**, 602–615.
- JAKIRLIĆ, S. & HANJALIĆ, K. 2002 A new approach to modelling near-wall turbulence energy and stress dissipation. *J. Fluid Mech.* **459**, 139–166.
- JAKIRLIĆ, S. & MADUTA, R. 2015 Extending the bounds of steady rans closures: Toward an instability-sensitive reynolds-stress model. *Int. J. Heat Fluid Flow* **51**, 175–194.
- JOVANOVIĆ, J. 2004 *The Statistical Dynamics of Turbulence*. Berlin [p]: Springer.
- JOVANOVIĆ, J., YE, Q. Y. & DURST, F. 1995 Statistical interpretation of the turbulent dissipation-rate in wall-bounded flows. *J. Fluid Mech.* **293**, 321–347.
- KASSINOS, S. C., REYNOLDS, W. C. & ROGERS, M. M. 2001 1-point turbulence structure tensors. *J. Fluid Mech.* **428**, 213–248.
- KHOURY, G. K. EL, SCHLATTER, P., NOORANI, A., FISCHER, P. F., BRETHOUWER, G. & JOHANSSON, A. V. 2013 DNS of turbulent pipe flow at moderately high Reynolds numbers. *Flow Turb. Comb.* **91**, 475–495.
- KIM, J. 1989 On the structure of pressure fluctuations in simulated turbulent channel-flow. *J. Fluid Mech.* **205**, 421–451.
- KIM, J. 2012 Progress in pipe and channel flow turbulence, 1961–2011. *J. Turb.* **13**, 000045(1–19).
- KIM, J., MOIN, P. & MOSER, R. 1987 Turbulence statistics in fully developed channel flow at low-Reynolds-number. *J. Fluid Mech.* **177**, 133–166.
- KOLOVANDIN, B. A. & VATUTIN, I. A. 1972 Statistical transfer theory in nonhomogeneous turbulence. *Int. J. Heat Mass Transfer* **15**, 2371–2383.
- LAI, Y. G. & SO, R. M. C. 1990 On near-wall turbulent flow modelling. *J. Fluid Mech.* **221**, 641–673.
- LAUNDER, B. E. & REYNOLDS, W. C. 1983 Asymptotic near-wall stress dissipation rates in a turbulent flow. *Phys. Fluids* **26** (5), 1157–1158.
- LAUNDER, B. E. & SHIMA, N. 1989 2-moment closure for the near-wall sublayer: Development and application. *AIAA J.* **27** (10), 1319–1325.
- LEE, M. & MOSER, R. D. 2015 DNS of turbulent channel flow up to $Re_\tau \approx 5200$. *J. Fluid Mech.* **774**, 395–415.
- LEE, M. J. & REYNOLDS, W. C. 1987 On the structure of homogeneous turbulence. In *Turbulent Shear Flows 5, Selected Papers for the 5. International Symposium on Turbulent Shear Flows, Cornell University, Ithaca [NY, USA], aug, 7–9, 1985* (ed. F. Durst, B. E. Launder, J. L. Lumley, F. W. Schmidt & J. H. Whitelaw), pp. 54–66. Berlin [DEU]: Springer.
- LOZANO-DURÁN, A. & JIMÉNEZ, J. 2014 Effect of the computational domain on direct simulations of turbulent channels up to $Re_\tau = 4200$. *Phys. Fluids* **26** (1), 011702(1–7).
- LUMLEY, J. L. 1978 Computational modeling of turbulent flows. *Adv. Appl. Mech.* **18**, 123–176.
- LUMLEY, J. L. & NEWMAN, G. R. 1977 The return to isotropy of homogeneous turbulence. *J. Fluid Mech.* **82**, 161–178.
- LUMLEY, J. L., YANG, Z. & SHIH, T. H. 1999 A length-scale equation. *Flow Turb. Comb.* **63**, 1–21.

- MANSOUR, N. N., KIM, J. & MOIN, P. 1988 Reynolds-stress and dissipation-rate budgets in a turbulent channel flow. *J. Fluid Mech.* **194**, 15–44.
- MARUSIC, I., MCKEON, B. J., MONKEWITZ, P. A., NAGIB, H. M., SMITS, A. J. & SREENIVASAN, K. R. 2010 Wall-bounded turbulent flows at high reynolds numbers: Recent advances and key issues. *Phys. Fluids* **22**, 065103(1–24).
- MARUSIC, I., MONTY, J. P., HULTMARK, M. & SMITS, A. J. 2013 On the logarithmic region in wall turbulence. *J. Fluid Mech.* **716**, R3(1–11).
- MATHIEU, J. & SCOTT, J. 2000 *An introduction to turbulent flow*. Cambridge [GBR]: Cambridge University Press.
- MONIN, A. S. & YAGLOM, A. M. 1971 *Statistical fluid mechanics: Mechanics of turbulence*, , vol. 1. Cambridge [MA, USA]: MIT Press.
- MOSER, R. D., KIM, J. & MANSOUR, N. N. 1999 Direct numerical simulation of turbulent channel flow up to $Re_\tau = 590$. *Phys. Fluids* **11** (4), 943–945.
- OBERLACK, M. 1997 Non-isotropic dissipation in non-homogeneous turbulence. *J. Fluid Mech.* **350**, 351–374.
- PATEL, V. C., RODI, W. & SCHEUERER, G. 1985 Turbulence models for near-wall and low-Reynolds-number flows: A review. *AIAA J.* **23**, 1308–1319.
- POPE, S. B. 2000 *Turbulent Flows*. Cambridge [GBR]: Cambridge University Press.
- RILEY, K. F., HOBSON, M. P. & BENICE, S. J. 2006 *Mathematical Methods for Physics and Engineering*, 3rd edn. Cambridge [GBR]: Cambridge University Press.
- RIVLIN, R. S. 1955 Further remarks on the stress-deformation relations for isotropic materials. *Indiana Univ. Math. J.* **4**, 681–702.
- RODI, W. & MANSOUR, N. N. 1993 Low Reynolds number k- ε modelling with the aid of DNS. *J. Fluid Mech.* **250**, 509–529.
- SCHULTZ, M. P. & FLACK, K. A. 2013 Reynolds-number scaling of turbulent channel flow. *Phys. Fluids* **25**, 025104(1–13).
- SCHUMANN, U. 1977 Realizability of Reynolds-stress turbulence models. *Phys. Fluids* **20**, 721–725.
- SILLERO, J. A., JIMÉNEZ, J. & MOSER, R. D. 2013 One-point statistics for turbulent wall-bounded flows at Reynolds numbers up to $\delta^+ \approx 2000$. *Phys. Fluids* **25**, 105102(1–16).
- SIMONSEN, A. J. & KROGSTAD, P. Å. 2005 Turbulent stress invariant analysis: Classification of existing terminology. *Phys. Fluids* **17**, 088103(1–4).
- SPEZIALE, C. G. 1989 Turbulence modeling in noninertial frames of reference. *Theor. Comp. Fluid Dyn.* **1**, 3–19.
- SPEZIALE, C. G. & GATSKI, T. B. 1997 Analysis and modelling of anisotropies in the dissipation rate of turbulence. *J. Fluid Mech.* **344**, 155–180.
- STEWART, G. W. 1998 *Matrix Algorithms I*. Philadelphia [PA, USA]: SIAM.
- TAGAWA, M., NAGANO, Y. & TSUJI, T. 1991 Turbulence model for the dissipation components of Reynolds stresses. 8. Symposium on Turbulence Shear Flows, Technical University of Munich [GER], paper 29-3.
- TAYLOR, G. I. 1938 Production and dissipation of vorticity in a turbulent fluid. *Proc. Roy. Soc. London A* **164**, 15–23.
- TAYLOR, J. R. 1997 *An Introduction to Error Analysis*. Sausalito [CA, USA]: University Science Books.
- TENNEKES, H. & LUMLEY, J. L. 1972 *A First Course in Turbulence*. Cambridge [MA, USA]: MIT Press.
- TOWNSEND, A. A. 1976 *The structure of turbulent shear flow*. Cambridge [GBR]: Cambridge University Press.
- VREMAN, A. W. & KUERTEN, J. G. M. 2014a Comparison of DNS databases of turbulent channel flow at $Re_\tau = 180$. *Phys. Fluids* **26**, 015102(1–21).
- VREMAN, A. W. & KUERTEN, J. G. M. 2014b Statistics of spatial derivatives of velocity and pressure in turbulent channel flow. *Phys. Fluids* **26**, 085103(1–29).
- VREMAN, A. W. & KUERTEN, J. G. M. 2016 A 3-order multistep time-discretization for a chebyshev tau spectral method. *J. Comp. Phys.* **304**, 162–169.